Engineering Fracture Mechanics 344 (2026) 112281

Contents lists available at ScienceDirect

Engineering Fracture Mechanics

journal homepage: www.elsevier.com/locate/engfracmech

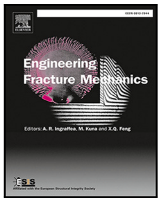

Comparative analysis of analytical-based micromechanical models for quasi-brittle materials

Pedro Henrique Rios Silveira *, Rita Esposito

Delft University of Technology, Netherlands

ARTICLE INFO

Keywords:
Anisotropic damage
Physics-based modeling
Mean-field homogenization
Linear elastic fracture mechanics
Unilateral effect

ABSTRACT

Micromechanical models offer a physics-based alternative to phenomenological approaches to simulate the behavior of quasi-brittle materials. By combining mean-field homogenization techniques with fracture mechanics principles, these models aim to capture anisotropic damage evolution, unilateral effects, and multiphysics coupling with a small number of inputs. However, despite their theoretical appeal, their practical application is often hindered by critical limitations. This paper presents a comprehensive and critical examination of micromechanical formulations, focusing on the influence of homogenization schemes, damage evolution criteria, and loading type in model response. It highlights key issues such as the limited accuracy of homogenization estimates at high crack densities, the instability of post-peak responses, spurious damage localization, and the challenges of modeling tensile-compressive asymmetry and non-homothetic crack growth. Through analytical derivations and numerical examples, the study demonstrates that many micromechanical models rely on assumptions that break down under more general conditions, leading to non-physical predictions outside the scope of model conception. The findings suggest that while micromechanical models are valuable in specific contexts, their broader applicability requires careful scrutiny and further development.

1. Introduction

Damage in quasi-brittle materials is widely accepted to arise from the propagation of pre-existing micro-cracks. Once these cracks become sufficiently large to interact with one another, they start to coalesce, eventually leading to macro-cracks. The problem of micro-crack growth and coalescence is complex. In part due to this complexity, the constitutive modeling of quasi-brittle materials, particularly in the context of structural analysis, is often done largely phenomenologically, meaning that a physical description of the microstructure of the material and its evolution is not attempted; rather, its macroscopic behavior is indirectly captured with little to no consideration of microstructural features.

In phenomenological models, the behavior of materials during loading is measured experimentally, and then a mathematical structure is proposed that captures such behavior. This provides a rather simple and flexible framework, since input parameters are directly related to experimentally measured quantities. Further, formulation details such as the shapes and evolution laws of limit surfaces can be modified in a flexible way to fit larger data sets. However, these models also have an important limitation: the physical meanings of their inputs can be tenuous or nonexistent, and the same is true for their internal variables.

In multiphysical models, this lack of physical meaning of internal and input variables often translates into multiple also phenomenological relationships between them and other (non-displacement) fields. These links are hard to establish, and the more

* Corresponding author.
E-mail address: P.H.RiosSilveira@tudelft.nl (P.H.R. Silveira).

https://doi.org/10.1016/j.engfracmech.2026.112281
Received 3 December 2025; Received in revised form 11 May 2026; Accepted 14 May 2026
Available online 28 May 2026

fields are added to the analysis, the larger the number of such relationships are needed. Further, phenomenological models make it harder to gain deeper insight into the behavior of coupled systems due to interactions having to be predetermined rather than emerging naturally.

The unclear connection between phenomenological internal variables and multiphysics fields, along with a desire to better capture complex interaction phenomena in quasi-brittle materials in an emergent way, was the main motivation for the development of a class of models based on a combination of fracture mechanics and homogenization theory applied to cracked-media. This framework is often referred to as 'Micromechanics', a nomenclature that is used in this work. Examples of multiphysics coupling of micromechanical models include, among others, the analysis of damage induced by the expansive byproducts of alkali-silica reactions in concrete [1–3] or by freezing of water inside rocks [4]; the ignition of explosive materials due to impact [5,6]; the weakening of the mechanical response of porous rocks due to the presence of water [7]; and the coupling of moisture diffusion and/or pore-pressure with damage evolution [8–11].

Authors of micromechanical models claim further advantages of this class of formulations, such as a more natural description of anisotropic damage evolution and its interaction with the initial anisotropy in the material itself [12]. Examples of this include embedding cracks into matrices that are initially transversely isotropic, such as shale [13], or orthotropic, such as masonry [14]. Another benefit is the direct modeling of crack-closure (the so-called 'unilateral' effect) [12,15,16] and the plasticity due to the sliding of these closed cracks [17–19]. Lastly, when these same mechanisms need to be accounted for in phenomenological-based models, they often require a large number of parameters. Hence, the limited number of input required in micromechanical models is also frequently cited as another main motivation for their use [10,14,18,20,21].

Despite the promising applications, the effectiveness of micromechanical models hinges on some important aspects: how reasonable are their predictions in comparison to experimentally-observed material behavior; how truly 'physical' are their input and internal variables; and how limited is their use in the context of numerical modeling of materials and structures under general loading conditions. To address these questions, this paper critically examines a number of micromechanical formulations with anisotropic damage evolution. First, an overview of the analyzed models is provided, with their formulations reported in a comparable format. This is done for the effective behavior of the cracked medium, the effect of contact between the crack surfaces, and the evolution of the damage state. Then, the paper shows how important choices such as the homogenization strategy and damage loading function profoundly affect the models' outputs, often in nonphysical ways. Lastly, some central aspects of the theory of micromechanics are put into question, such as its ability to represent the tensile-compressive asymmetry of quasi-brittle materials, the accuracy of its post-peak behavior, and the validity of its assumed crack shapes and distributions, particularly during damage evolution.

Some novelties of this work include a formal demonstration of the equivalence between models that were previously treated as separate, a more general discussion of the stability of the softening curves under damage evolution than what is provided in literature, a large collection of examples of softening curves for different combinations of damage-resistance function and homogenization schemes, and an initial description of a pathological phenomenon of spurious localization. The paper also draws attention to the fact that many models show incorrect softening responses under certain load conditions, and/or rely on a fast increase in the density of cracks to values beyond the range where mean-field homogenization theory can be reasonably considered applicable.

To aid reading, a list of symbols and nomenclatures is provided in Table 1.

2. Effective behavior of cracked media

Micromechanical approaches are formulated based on at least two principles. On one side, homogenization techniques are used to evaluate the effective stiffness tensor of the damaged medium. On the other side, damage increases under evolution laws, which are often based on principles of linear fracture mechanics. In this section, the general formulations are reported for the former case.

2.1. Effective stiffness tensor for the case of open cracks

There are broadly two classes of Eshelby-based analytical homogenization techniques, fundamentally distinguished by their choice of reference medium: 'effective medium' schemes and 'effective field' (often referred to as 'mean-field') schemes. In effective medium theories, inclusions are assumed to be embedded directly into an unknown, homogenized medium with effective properties. Because the reference medium itself depends on the solution, the homogenization problem is implicitly defined and must generally be solved either iteratively or incrementally. In this work, the focus is on anisotropic damage, where cracks can grow independently in multiple directions. Under these general conditions, closed-form expressions cannot be readily obtained from implicit effective medium theories, which greatly complicates the formulation of micromechanical models. Hence, these techniques will not be discussed, though it should be highlighted that they remain applicable in the case of simple crack distributions, such as parallel cracks or isotropic distributions of simultaneously growing cracks. For more information on effective medium techniques for cracked media, the reader is pointed to Kachanov [22,23].

In contrast, mean-field homogenization techniques assume that inclusions are embedded into the virgin, undamaged matrix. Rather than interacting with an unknown effective medium, these inclusions are assumed to be subjected to 'effective' (volume-averaged) stress or strain fields acting on the matrix phases. By applying the volume averaging principle over a Representative Volume Element (RVE), the macroscopic stress and strain are defined as the volume-weighted averages of the microscopic fields of the constituent phases [24–26]. Substituting the phase-wise constitutive relations into the averaged stress expression, and

Table 1
Table of symbols and nomenclature used throughout this work.

Symbol	Description
Fourth-order tensors	
$\mathbb{C}$, $\mathbb{D}$	Stiffness and compliance tensors
$\mathbb{I}$, $\mathbb{O}$	Fourth-order identity and null tensors
$\mathbb{S}$, $\mathbb{A}$	Eshelby tensor and strain concentration tensors for any estimate other than Dilute
$\mathbb{T}$, $\overline{\mathbb{T}}$	Dilute strain concentration tensor and its equivalent for vanishing aspect ratios
$\mathbb{M}$	Scaled version of $\overline{\mathbb{T}}$, related to the crack strains in the Dilute estimate
$\mathbb{H}$	Auxiliary compliance-like tensor, related to the crack strains in the MT estimate
Second-order tensors	
$\boldsymbol{\Sigma}$, $\boldsymbol{E}$	Macroscopic stress and strain tensor
$\boldsymbol{\sigma}$, $\boldsymbol{\epsilon}$	Local stresses and strains of each crack family
Scalars	
ϕ	Volume fractions of different phases
$\mathcal{N}^c$	Number of cracks per unit volume
a, c, X, s^c, V^c	Radius, thickness, aspect ratio, surface area, and volume of the cracks
$\mathcal{E}$	Adimensional crack density parameter
E, ν, G	Young's modulus, Poisson's ratio, and shear modulus
μ, μ_d	Friction coefficient and slope of the Mohr–Coulomb limit surface
γ	Surface energy
K^I, K^{Ic}	Mode-I stress intensity factor and fracture toughness
α	Used for scalar factors of different kinds
k	Used for constants of various kinds
f_t, f_c, f_s	Tensile, compressive, and shear strengths
Functions	
f, g, q	Used to denote functions or various kinds
$\mathcal{F}$, $\mathcal{R}$	Damage driving force and resistance functions
ψ	Energy densities of various kinds
Superscripts	
$\circ$	Open cracks
$*$	Closed cracks without friction between the crack surfaces
$\circ\|*$	Cracks that are either open, or closed without friction
c	Cracks in any state, including with friction
μ, d	Quantities related to friction or damage
D	Related to the statistical distribution of cracks
N	Normal component of a quantity with respect to the plane of a crack
T	Lateral/tangential component of a quantity with respect to the plane of a crack
E, Σ, h	Related to the macrostrains, the macrostresses, or the homogenized medium
(D), (MT), (PCW)	Related to the Dilute, Mori–Tanaka, and Ponte-Castaneda-Willis estimates
Abbreviations	
MT	Mori–Tanaka homogenization scheme/estimate
PCW	Ponte-Castañeda-Willis homogenization scheme/estimate
RVE	Representative Volume Element
LCP	Linear Complementarity Problem
LEFM	Linear Elastic Fracture Mechanics

introducing strain concentration tensors to relate the average strain in each inclusion family to the macroscopic strain, the effective stiffness tensor of a heterogeneous material with N families of inclusions can be written, in general form, as [26]:

$$\mathbb{C}^h = \mathbb{C}^m + \sum_{i=1}^{N} \phi_i^\beta \left(\mathbb{C}_i^\beta - \mathbb{C}^m \right) : \mathbb{A}_i^\beta \tag{1}$$

where $\mathbb{C}^h$, $\mathbb{C}^m$, $\mathbb{C}_i^\beta$ are the stiffness tensors of the homogenized (h) material, the matrix (m), and of the ith family of inclusions (β); $\mathbb{A}_i^\beta$ are the so-called 'strain concentration' tensors of the ith inclusion family, which map the macroscopic strain to the average local strain in the inclusions; and ϕ_i^β is the volume fraction of the ith inclusion family. For more details about the derivation of Eq. (1), the reader is pointed to Ref. [26].

Various mean-field techniques are available in the literature, each working with a different set of assumptions to calculate the effective fields acting in the inclusions. Three notable schemes for which there are closed-form expressions for the concentration tensors ($\mathbb{A}_i^\beta$) are the Dilute (D), Mori–Tanaka (MT) [27–29], and Ponte-Castaneda-Willis (PCW) [30] estimates. The Dilute estimate follows directly from the 'Eshelby inclusion problem' [31] and its concentration tensor was given by Hill [24]. Since this concentration tensor appears in the other estimates as well, it is given the special symbol $\mathbb{T} = \mathbb{A}^{(Dilute)}$. Under the assumption that the inclusion dispersion is so diluted that each individual inclusion in each family can be considered completely isolated and embedded in an infinite medium under remote fields matching the RVE averages, this tensor reads as:

$$\mathbb{T}_i^{\beta} = \left[\mathbb{I} + \mathbb{S}_i^{\beta} : \mathbb{D}^m : \left(\mathbb{C}_i^{\beta} - \mathbb{C}^m\right)\right]^{-1} \tag{2}$$

where $\mathbb{I}$ is the fourth-order identity tensor, and $\mathbb{S}_i^{\beta}$ is the so-called 'Eshelby tensor' of the ith inclusion family. The Eshelby tensor maps the uniform eigenstrain of an inclusion to the resulting constrained strain, explicitly accounting for the elastic confinement imposed by the surrounding matrix. As such, it serves as the primary building block for homogenization schemes. General expressions for this tensor, along with specific cases of interest, can be found in Mura [25].

For the particular case of void inclusions ($\mathbb{C}_i^{\beta} = \mathbb{O}$), the effective stiffness of the homogenized medium can be written more simply as:

$$\mathbb{C}^{\circ} = \mathbb{C}^m - \mathbb{C}^m : \sum_{i=1}^{N} \phi_i^c \mathbb{A}_i^{\circ} \tag{3}$$

which follows directly from Eq. (1). While this expression is valid for voids of any shape, they will henceforth be referred to as 'cracks'. The $\{\cdot\}^{\circ}$ notation refers specifically to the case of *open* cracks (closed cracks are discussed next), with $\{\cdot\}^c$ referring to either generalized quantities, or those that are naturally independent of the state of the crack. This open crack assumption results in a Dilute concentration tensor of form:

$$\mathbb{T}_i^{\circ} = \left(\mathbb{I} - \mathbb{S}_i^{\circ}\right)^{-1} \tag{4}$$

which also follows directly from Eq. (2) under the assumption of null inclusion stiffness.

So far, no assumption has been made regarding the shapes of cracks. In this general case, the volume fraction of the ith crack family (ϕ_i^c) can be expressed as:

$$\phi_i^c = \mathcal{N}_i^c V_i^c \tag{5}$$

where $\mathcal{N}_i^c$ is the number of cracks per unit volume of material for the ith crack family, with V_i^c being the volume of each individual crack in the family. However, in order to define an expression for V_i^c, cracks are now assumed to be flat and circular ellipsoids, such that their semi-axes obey the relation $a = b \gg c$. These are so-called 'penny-shaped' cracks and lead to the expression:

$$V_i^c = \frac{4\pi}{3} c_i a_i^2 = \frac{4\pi}{3} X_i a_i^3 \tag{6}$$

where a_i is the radius of the crack and c_i is half of its thickness. $X_i = c_i/a_i$ is the aspect ratio of the penny-shaped cracks. Eshelby's key insight was that, in the case of ellipsoidal inclusions, the $\mathbb{S}$ tensors are constant. Since penny-shaped cracks are a special case of an ellipsoid, this also leads to constant Dilute concentration tensors $\mathbb{T}_i^{\circ}$. This property is fundamental to the development of analytical micromechanics.

Here, it is useful to introduce the so-called 'crack-density' parameter, defined as $\mathcal{E}_i = \mathcal{N}_i a_i^3$. The crack-density parameter is an adimensional quantity that sees ample use as the damage-driving variable in many formulations and was first proposed by Bristow [32] and later generalized by Budiansky and O'Connell [33]. Notably, this quantity is independent of the aspect ratio and tends to be more appropriate to describe cracked microstructures where the cracks have small to vanishing thickness and contribute little to nothing to the void fraction of the composite [23]. In terms of this parameter, the volume fraction of cracks can be rewritten as:

$$\phi_i^c = \frac{4\pi}{3} \mathcal{E}_i X_i \tag{7}$$

Another quantity that is useful to write as a function of the crack-density parameter is the surface area of a crack family, which can be approximately expressed as:

$$s_i^c = 2\pi \mathcal{N}_i a_i^2 = 2\pi \mathcal{N}_i \left(\frac{\mathcal{E}_i}{\mathcal{N}_i}\right)^{\frac{2}{3}} = 2\pi \mathcal{N}_i^{\frac{1}{3}} \mathcal{E}_i^{\frac{2}{3}} \tag{8}$$

It should be noted that this approximation for the crack surface also relies on the aspect ratio being small (flat circular cracks). The limit of this case, where the aspect ratio is vanishing, is of particular importance to analytical micromechanical models. In this scenario, the crack volume vanishes as well. However, the $X_i \mathbb{T}_i^{\circ}$ product remains finite, since $\mathbb{T}_i^{\circ}$ has terms in the order of $1/X_i$. Therefore:

$$\lim_{X_i \to 0} X_i \mathbb{T}_i^{\circ} = \overline{\mathbb{T}}_i^{\circ} \tag{9}$$

where $\overline{\mathbb{T}}_i^{\circ}$ is now *independent* of the (vanishing) aspect ratio. The existence of this limit and its format have been discussed in Refs. [1,34,35], among others.

Under the assumption of vanishing aspect ratio (and, therefore, of vanishing void fraction), the homogenized stiffness and compliance tensors of the three chosen estimates (Dilute, MT, and PCW) are given in Table 2. In the expressions in this table, $\mathbb{D}^m$ is the compliance tensor of the matrix ($\mathbb{D}^m = (\mathbb{C}^m)^{-1}$), and the following compliance-like auxiliary tensor is defined:

$$\mathbb{H}_i^{\circ} = \mathbb{M}_i^{\circ} : \mathbb{D}^m \tag{10}$$

Table 2
Effective stiffness and compliance tensors for the case of open penny-shaped cracks.

	Effective stiffness tensor ($\mathbb{C}^h$)	Effective compliance tensor ($\mathbb{D}^h$)
(D)	$\mathbb{C}^m : \left(\mathbb{I} - \sum_{i=1}^N \mathcal{E}_i \mathbb{M}_i^\circ\right)$	$\mathbb{D}^m : \left(\mathbb{I} - \sum_{i=1}^N \mathcal{E}_i \mathbb{M}_i^\circ\right)^{-1}$
(MT)	$\mathbb{C}^m : \left(\mathbb{I} + \sum_{i=1}^N \mathcal{E}_i \mathbb{M}_i^\circ\right)^{-1}$	$\mathbb{D}^m + \sum_{i=1}^N \mathcal{E}_i \mathbb{H}_i^\circ$
(PCW)	$\mathbb{C}^m : \left\{\mathbb{I} - \left[\left(\sum_{i=1}^N \mathcal{E}_i \mathbb{M}_i^\circ\right)^{-1} + \mathbb{S}^D\right]^{-1}\right\}$	$\mathbb{D}^m : \left\{\mathbb{I} - \left[\left(\sum_{i=1}^N \mathcal{E}_i \mathbb{M}_i^\circ\right)^{-1} + \mathbb{S}^D\right]^{-1}\right\}^{-1}$

with:

$$\mathbb{M}_i^\circ = \frac{4\pi}{3}\overline{\mathbb{T}}_i^\circ \tag{11}$$

simply being a scaled version of the Dilute concentration tensor $\overline{\mathbb{T}}_i^\circ$, with the scaling factor of $4\pi/3$ emerging from the volume expression in Eq. (7).

For details regarding the expressions in this table, the reader is also pointed to Ref. [8]. Here, it suffices to highlight that $\mathbb{S}^D$ is *not* the Eshelby tensor of the crack shape, as is the case for the $\mathbb{S}_i^\circ$ tensors in Eq. (4). Rather, it is defined in terms of the statistical *distribution* of cracks — hence the superscript $\{\cdot\}^D$. Therefore, inclusions can be assumed to be distributed inside the matrix in a number of ways.

Using the PCW estimate, both the Dilute and MT expressions can be recovered by setting $\mathbb{S}^D = \mathbb{O}$ and $\mathbb{S}^D = \mathbb{I}$ respectively. For the Dilute method, this implies no crack distribution at all — the estimate follows directly from the Eshelby problem under the assumption of a single inclusion inside an infinite matrix. As for the MT estimate, the interpretation is that the method implicitly assumes that the statistical distribution of inclusions in the matrix follows the inclusion shape itself, as pointed out by several authors [30,36,37]. For penny-shaped cracks, this leads to the identity tensor.

In this paper, when the PCW estimate is used, it is assumed that the initial distribution of the penny-shaped cracks is spherical. Hence, the centers of the cracks are dispersed isotropically, and $\mathbb{S}^D$ is also an isotropic tensor (see Ref. [25] for the expression for the Eshelby tensors in the spherical case). This essentially corresponds to randomly placed inclusions with no distribution bias.

An important detail worth highlighting is that the Dilute method has two forms: the stiffness-based and the compliance-based estimates, whose inverses do not equal each other. In the case of cracks with vanishing aspect ratios, the compliance-based approximation yields the same expression as that of the MT estimate. This is directly caused by the fact that (for such vanishing ratios) the effective and the macroscopic stresses in the cracked medium are equal. In other words, volumeless penny-shaped cracks do not change the average stress in the matrix [22,23]. Hence, the MT assumption that the inclusion is surrounded by an atmosphere of matrix under mean stresses is essentially equivalent to the compliance-based Dilute assumption that the matrix is under the far-field stresses. This equality is precisely what eliminates the effect of the interactions between the inclusion families, which is normally present in the MT estimate.

The equivalence between the MT method and the compliance-based Dilute approach seems to have been first noted by Benveniste [28] and is discussed in more detail in Refs. [22,38], which further confirmed it to the case of closed microcracks. Notably, such equivalence is the source of confusion in micromechanics literature, where the term 'Dilute' is often used without specification of whether its compliance or stiffness form is used. To avoid this confusion, the authors of this work further reinforce that the 'Dilute' term is being used here *exclusively* for the stiffness-based estimate. The compliance-based Dilute and MT estimates are referred to as 'non-interacting' approximations by some authors.

2.2. Effects of crack closure

So far, the discussions in this work have been limited to the case of open cracks. However, as demonstrated by different authors [15,35,39], closed, frictionless cracks can be treated in a similar framework. In the limit-case of vanishing aspect ratios, this can be achieved by replacing the $\overline{\mathbb{T}}_i^\circ$ tensors with a version where only the shear terms are considered, which in this work is notated as $\overline{\mathbb{T}}_i^*$, with superscript $*$ indicating closed, frictionless cracks. Hence, a generalized $\overline{\mathbb{T}}_i^{*|\circ}$ tensor can be written as:

$$\overline{\mathbb{T}}_i^{*|\circ} = \begin{cases} \overline{\mathbb{T}}_i^\circ & \text{if open} \\ \overline{\mathbb{T}}_i^* & \text{if closed} \end{cases} \tag{12}$$

Open cracks are considered to have a positive normal component of the traction vector acting on their plane, hence: $\sigma_i^N = \hat{\boldsymbol{n}}_i \cdot \boldsymbol{\Sigma} \cdot \hat{\boldsymbol{n}}_i \geq 0$, with $\hat{\boldsymbol{n}}_i$ being the unit vector normal to the crack plane. For closed cracks, the component is negative ($\sigma_i^N < 0$).

The physical meaning behind the vanishing of the normal terms in $\overline{\mathbb{T}}_i^*$ is simple: in closed cracks, their normal contribution to the behavior of the effective medium should vanish, since there is perfect transfer of normal stresses across the crack surfaces. Therefore, from the perspective of the normal crack directions, the homogenized medium does not 'see' the closed cracks. Following this logic, the format for $\overline{\mathbb{T}}_i^*$ can be obtained by replacing the void inclusion by a fictitious material with null shear strength and an arbitrary (finite) bulk strength. Then, taking the limit of this fictitious inclusion when the aspect ratio vanishes, analogously to the case of open cracks, yields the tensor $\overline{\mathbb{T}}_i^*$, which has no dependency on the specific value of the bulk modulus in the effective material (as long as it is finite). This procedure seems to have been first described in Refs. [15,39] and is discussed in more detail in Ref. [35]. The specific form of the $\overline{\mathbb{T}}$ tensors for both open and closed cracks can be obtained in these references for the case of an isotropic matrix.

It should be highlighted that open/sliding penny-shaped cracks will be subjected to large deformations. In principle, these deformations will change the aspect ratio of the cracks in a load-dependent way. Consequently, the more general $\mathbb{T}_i$ tensors are also load-dependent, which means the problem has to be solved incrementally. However, this non-linearity also vanishes in the case of vanishing aspect ratios, as discussed in Ref. [35]. Hence, the constant tensors $\overline{\mathbb{T}}_i$ can be used in a load-independent way. For this reason, among others that will be discussed next, the rest of this work assumes cracks with vanishing aspect ratios, except when explicitly noted.

2.3. Effects of local friction

Several literature models are formulated without considering the effects of local friction between the crack surfaces (e.g. Refs. [2,3,12,15,16,40–45]). In these cases, the expressions defined in the previous sections are generally sufficient to characterize the behavior of the cracked medium for a given distribution of crack families. However, many models also include the effects of local friction into their formulations, in one form or another. Since friction is a dissipative process, it requires its own evolution equations. This case is briefly discussed in this section. Further, more detailed descriptions of select frictional formulations are given in Annex A.

An underlying assumption of local friction is that the effects of each crack family on the homogenized medium can be replaced by an equivalent strain acting on an uncracked matrix. Under this hypothesis, the constitutive law can be written as:

$$\boldsymbol{\Sigma} = \mathbb{C}^m : (\boldsymbol{E} - \boldsymbol{E}^c) \tag{13}$$

where $\boldsymbol{E}^c$ is the *total* crack-strain contribution, which, for now, assumes open cracks, such that $\boldsymbol{E}^c = \boldsymbol{E}^\circ$. For this case (of open cracks), the constitutive law can also be directly expressed using the homogenized stiffness tensors defined in Eq. (3), such that:

$$\boldsymbol{\Sigma} = \mathbb{C}^\circ : \boldsymbol{E} \tag{14}$$

These two equations can only be satisfied simultaneously if a compatibility constraint is imposed in the form:

$$\boldsymbol{E}^\circ = \left(\mathbb{D}^\circ - \mathbb{D}^m\right) : \boldsymbol{\Sigma} = \left(\mathbb{D}^\circ - \mathbb{D}^m\right) : \mathbb{C}^\circ : \boldsymbol{E} \tag{15}$$

Assuming that the cracks can have non-vanishing aspect ratios and combining Eq. (15) with the formula for $\mathbb{C}^\circ$ obtained from Eq. (3) results in:

$$\boldsymbol{E}^\circ = \sum_{i=1}^{N} \phi_i^c \mathbb{A}_i^\circ : \boldsymbol{E} = \sum_{i=1}^{N} \phi_i^c \mathbb{A}_i^\circ : \mathbb{D}^\circ : \boldsymbol{\Sigma} \tag{16}$$

If the following notation is then introduced:

$$\boldsymbol{E}^\circ = \sum_{i}^{N} \boldsymbol{\epsilon}_i^\circ \tag{17}$$

such that $\boldsymbol{\epsilon}_i^\circ$ are the individual crack family contributions, this naturally leads, by direct comparison with Eq. (16), to:

$$\boldsymbol{\epsilon}_i^\circ = \phi_i^c \mathbb{A}_i^\circ : \boldsymbol{E} = \phi_i^c \mathbb{A}_i^\circ : \mathbb{D}^\circ : \boldsymbol{\Sigma} \tag{18}$$

For most homogenization schemes, the contributions of each crack family are functions of the states of all the other crack families in both the stress and strain forms of Eq. (18). This is because the individual contributions of each family to the compliance tensor or its product with the strain concentration tensor are not linear - a consequence of the interaction between families that is inherent to most homogenization schemes. The two exceptions are the Mori–Tanaka estimate with vanishing crack thickness, such that the matrix volume fraction remains unitary, and the stiffness-based Dilute estimate more generally. In these cases, then:

$$\boldsymbol{\epsilon}_i^{\circ(D)} = \mathcal{E}_i \mathbb{M}_i^\circ : \boldsymbol{E} \quad ; \quad \boldsymbol{\epsilon}_i^{\circ(MT)} = \mathcal{E}_i \mathbb{H}_i^\circ : \boldsymbol{\Sigma} \tag{19}$$

Notably, the $\boldsymbol{\epsilon}_i^\circ$ contributions are linearly dependent on the damage parameter for the Mori–Tanaka estimate in stress form and for the Dilute estimate in strain form, which can again be traced to the equivalence between the compliance-based Dilute estimate and the MT one for the case of penny-shaped cracks with vanishing aspect ratios that was previously discussed.

In the vast majority of micromechanical models, local friction is then introduced to the MT version of Eq. (19), partially due to its stress-linearity. To do so, a local friction contribution term is added to this equation as follows:

$$\boldsymbol{\epsilon}_i^c = \mathcal{E}_i \mathbb{H}_i^\circ : \left(\boldsymbol{\Sigma} - \boldsymbol{\sigma}_i^\mu\right) \tag{20}$$

where $\boldsymbol{\sigma}_i^\mu$ is the local stress contribution due to both crack closure and friction, and $\boldsymbol{\epsilon}_i^c$ are the generalized contributions of the ith crack family. From this general format, different frictional formulations are then characterized by their specific choice of expression for the $\boldsymbol{\sigma}_i^\mu$ local friction term. Three notable examples are the local plasticity approach of Zhu and collaborators [16,17,19,46,47]; the simplified locally-explicit stress-rate approach proposed by researchers at Los Alamos [6,48]; and the fully explicit strain-based formulation included in the model by Jefferson and Bennett [49,50]. In this section, these approaches will be briefly described. For more details, the reader is referred to the Annex A.

In the local plasticity approach, the local frictional stresses $\boldsymbol{\sigma}_i^{\mu}$ in Eq. (20) are isolated and made to satisfy a sliding condition, which is achieved by determining (potentially many) plastic multipliers under a local flow rule for the increments in the $\boldsymbol{\epsilon}_i^c$ local strains. This is an implicit procedure at the local level, somewhat analogous to 'classic' multi-surface plasticity. However, it is more complicated to solve than standard plasticity, with the macrostress acting as a back-stress term in all the local plasticity problems, thus coupling them (see Refs. [16,17,19,46]). The flow rule can be non-associated, which allows dilatancy to occur at a prescribed rate. Further, since the sliding conditions are satisfied strictly using a Linear Complementarity Problem (LCP), friction is rigorously modeled.

In the Los Alamos model, on the other hand, the rate of change of the crack strains ($\dot{\boldsymbol{\epsilon}}_i^c$) is considered directly proportional to the rate of change of the macrostress $\dot{\boldsymbol{\Sigma}}$. The proportionality between these variables is then written purely in terms of the components of macrostress ($\boldsymbol{\Sigma}$). Locally, the procedure is now explicit. Globally, however, $\boldsymbol{\Sigma}$ is still implicitly defined. In the Los Alamos works, this dependency is addressed via explicit time integration, thus rendering the entire procedure fully explicit. No dilatancy is considered, and friction is modeled in an approximate sense, since the LCP problem is no longer being strictly enforced.

Lastly, in the model by Jefferson and Bennett, the local frictional stresses ($\boldsymbol{\sigma}_i^{\mu}$) are written directly in terms of the macro*strains* ($\boldsymbol{E}$), rather than macro*stresses*. With some additional assumptions, this in turn allows for the $\boldsymbol{\epsilon}_i^c$ strains to also be written explicitly in terms of the macrostrains. As such, a nonlinear, strain-dependent homogenized stiffness tensor can be formed, rendering the entire procedure fully explicit by default. Friction is considered to be the result of mechanical interlock between the crack surface asperities, which are approximated as being 'cone-like'. In order for the cracks to slide, the asperities have to physically move over one another. This results in significant dilatancy, which is a direct consequence of the shapes of the cone. Contact can even happen under a (small) positive strain component perpendicular to the crack plane. In other words, friction can still occur in what other formulations would consider 'open' cracks.

Apart from these local formulations, many authors [4,21,51–60] resort instead to solving the plasticity problem at the global level. In these cases, a macroscopic version of the local frictional stress is defined, and the flow rule gives a global rather than local strain increment. These models are not discussed in this work.

3. Damage evolution criteria

So far, the formulations presented in this work have been outlined for a given damage state; hence, damage evolution laws now need to be discussed. In micromechanical approaches, this is done in three different ways. One is to use energy-based approaches, often formulated within the framework of thermodynamics. This appears to be the most popular technique (e.g. Refs. [2,15,17,35,61,62]). Another way is to use tractions in the crack plane to formulate the damage condition. This is often done using expressions derived from Linear Elastic Fracture Mechanics (LEFM). Examples include expressions derived from energetic considerations, such as the one used by the 'SCRAM' model from the Los Alamos laboratory [5,6], or from stress-intensity factors, such as the expressions used by Iskhakov et al. [3]. Lastly, damage evolution can also be formulated purely phenomenologically in terms of the components of the *strain*, rather than the stress tensor, as in the model by Jefferson and Bennett [49,50]. All these cases are discussed in this section.

Regardless of the choice of the variable driving the damage, damage evolution laws in micromechanical models are often based on a few key assumptions:

- The growth of the cracks is homothetic: the cracks remain both planar and circular.
- The coalescence of cracks is generally not (directly) considered: when it is an explicit model input, the number of cracks per unit volume in each crack family remains constant during damage evolution, and their radii evolve smoothly. Further, many models use only the crack density parameter, without any consideration for the actual number of cracks.
- Each cracking direction is represented by a single damage parameter. In principle, while statistical crack distributions could be considered and damage could evolve differently across the spectra of crack sizes, this is not addressed in the application and validation of most models, which are only formulated in terms of one internal variable per crack family — either a characteristic radius or a single crack density parameter (or related transformed damage variable).
- Crack localization is not considered via the homogenization framework: all cracks in a family are assumed to grow together and by the same amount.

With these assumptions in mind, the damage evolution process can be written, in a generic form, as:

$$f_i^d = \mathcal{F}_i - \mathcal{R}_i \leq 0 \tag{21}$$

where f_i^d is the damage-loading function of the ith crack family, $\mathcal{F}_i$ is the damage driving 'force', and $\mathcal{R}_i$ the 'resistance' to damage propagation.[1] Based on this damage-loading function, damage evolves according to a LCP of form:

$$f_i^d \leq 0 \qquad d\mathcal{X}_i \geq 0 \qquad f_i^d d\mathcal{X}_i = 0 \tag{22}$$

[1] This format for the damage-loading function and its associated nomenclature is usually present only in energy-based models and has roots in thermodynamics. In this work, it is extended to the other types of damage-evolution law. Nevertheless, f_i^d can also be formulated directly, without being split into 'driving' and 'resisting' terms. This is particularly the case in purely phenomenological models.

where $\mathcal{X}_i$ are the chosen damage variables, generally (but not necessarily) the crack-density parameters $\mathcal{E}_i$. Solutions to this LCP often take the form of a return-mapping algorithm with an associated damage potential. Nevertheless, other choices are possible, such as return-mapping with non-associated potentials [41], or a radial-return algorithm in stress-space [2,63].

3.1. Energy-based evolution criteria

For the energy-based damage models, the free energy density stored in the deformed material is what drives the damage process. Therefore, an expression for this energy needs to be defined. For a homogenized cracked medium (h), this can be achieved by summing two terms: the elastic contribution of the deformed matrix to the energy (m), and the contribution of the energy stored in the sliding/opening cracks (c) [17,47,64]. Therefore:

$$\psi^h = \psi^m + \psi^c \tag{23}$$

This splitting is directly related to the fact that an elastic body loaded at the boundary and containing traction-free penny-shaped cracks is equivalent (in mean effective terms) to that of a body where fictitious tractions are applied to the crack faces and the boundary is traction free instead [22]. The matrix contribution can be expressed as:

$$\psi^m = \frac{1}{2}(\boldsymbol{E} - \boldsymbol{E}^c) : \mathbb{C}^m : (\boldsymbol{E} - \boldsymbol{E}^c) \tag{24}$$

where $\boldsymbol{E} - \boldsymbol{E}^c$ has the meaning of an 'effective' strain acting on an uncracked (elastic) material. This effective strain is such that it yields the same stress as that of the total strain $\boldsymbol{E}$ acting on the effective (cracked) system — hence the stiffness tensor $\mathbb{C}^m$ being used. As for the ψ^c contribution, it can be given as [17,47,64]:

$$\psi^c = \frac{1}{2}\sum_{i=1}^{N} \boldsymbol{\epsilon}_i^c : \left(\boldsymbol{\Sigma} - \boldsymbol{\sigma}_i^\mu\right) \tag{25}$$

which has the meaning of the work done by the effective stress $\boldsymbol{\Sigma} - \boldsymbol{\sigma}_i^\mu$ over the displacement jumps between the crack surfaces given by $\boldsymbol{\epsilon}_i^c$. For the MT estimate in particular, this term can be equivalently given as:

$$\psi^{c(MT)} = \frac{1}{2}\sum_{i} \boldsymbol{\epsilon}_i^c : (\mathcal{E}_i \mathbb{H}_i^\circ)^+ : \boldsymbol{\epsilon}_i^c \tag{26}$$

which comes from inverting Eq. (20) and replacing the resulting expression over the $\boldsymbol{\Sigma} - \boldsymbol{\sigma}_i^\mu$ terms. The $\{\cdot\}^+$ operator is the Moore–Penrose inverse, which is used because $(\mathbb{H}_i^\circ)^+$ is rank-deficient. This format is far more useful, since the macrostress-dependency vanishes, such that $\psi^h = \psi^E(\boldsymbol{E}, \mathcal{E}_i, \boldsymbol{\epsilon}_i^c)$ is the Helmholtz free energy density, with $\boldsymbol{\epsilon}_i^c$ being treated as internal state variables.

Another (stronger) simplification can be obtained for the case of frictionless sliding. When friction and its associated evolution equations are not present, the Helmholtz free energy density can be directly written using the effective stiffness tensor, yielding:

$$\psi^E = \frac{1}{2}\boldsymbol{E} : \mathbb{C}^{*|\circ} : \boldsymbol{E} \tag{27}$$

where $\mathbb{C}^{*|\circ}$ is assembled considering that each crack family can be assumed either open or sliding without friction (see the $\overline{\mathbb{T}}_i^{*|\circ}$ tensor in Eq. (12)). Lastly, another possibility introduced by Esposito and Hendriks [2] is to consider no crack closure/friction at all and use only the positive part of the macroscopic strain tensor to drive damage evolution. This approach also appears in Vu et al. [43] and is inspired by the well-known concrete model by Mazars [65].

The energy expressions discussed so far are based on the macrostrains as the prescribed variable. This format is particularly useful for the solution of micromechanical models using discretized numerical schemes, where the strains are often the prescribed quantities (such as a constitutive subroutine for a Finite Element Analysis software, for instance). However, it will also prove relevant for this work to express another (equivalent) energy in terms of stresses — the so-called Gibbs free energy density ψ^Σ. It suffices to show the simplified expression that can be used for the case of frictionless cracks, which reads as:

$$\psi^\Sigma = \frac{1}{2}\boldsymbol{\Sigma} : \mathbb{D}^{*|\circ} : \boldsymbol{\Sigma} \tag{28}$$

The Gibbs free energy density can also be expressed for the case of frictional cracks (e.g. Ref. [47]), but this is not necessary for this work. The Gibbs and Helmholtz free energy density are connected by the Legendre transformation. With either of the two, the driving force can then be expressed as:

$$\mathcal{F}_i = -\partial_{\mathcal{E}_i}\psi^E = \partial_{\mathcal{E}_i}\psi^\Sigma \tag{29}$$

Additionally, the following dual equations are also valid:

$$\boldsymbol{\Sigma} = \partial_{\boldsymbol{E}}\psi^E \quad ; \quad \boldsymbol{E} = \partial_{\boldsymbol{\Sigma}}\psi^\Sigma \tag{30}$$

While this work is focused primarily on anisotropic damage, where multiple independent crack families are generally present, it is highlighted that other approaches also exist. As an example, the models in Refs. [2,3,42,43] rely on 3 orthogonal crack families (and therefore an inherently orthotropic damage evolution). Similarly, isotropic damage models, where a single damage parameter is employed, are also very popular [4,19,21,51–60,62,66,67]. In these models, no crack family discretization is employed.

3.2. Stress-based evolution criteria

Stress-based laws for micromechanical models are often derived based on principles of LEFM. One example of this approach is the SCRAM formulation [5,6]. From the stability analysis of a single penny-shaped crack in an infinite elastic and isotropic medium, based on the Griffith energy-balance, a limit function can be derived of form:

$$f_i = \frac{8}{3}\frac{1-\nu}{2-\nu}\frac{1}{G}q_i^\sigma - \mathcal{R}_i \leq 0 \tag{31}$$

where G is the shear modulus and ν is the Poisson's ratio of the elastic medium. The first term in this expression is the driving force, with q_i^σ being written as:

$$q_i^\sigma = \begin{cases} \left(1-\frac{\nu}{2}\right)\left(\sigma_i^N\right)^2 + \left(\sigma^T\right)^2 & \text{(open)} \\ \left\langle \sigma^T + \mu\sigma_i^N \right\rangle^2 & \text{(closed)} \end{cases} \tag{32}$$

where μ is the friction coefficient, σ_i^N the (signed) normal component of the traction on the crack plane, and σ^T the magnitude of the shear traction on the crack plane. The $\langle\cdot\rangle$ operators are the Macaulay brackets, used to denote the ramp function.

The expression for q_i^σ in the case of open cracks was derived by Keer [68], while the one for closed sliding cracks was originally proposed by Dienes [69] with an incorrect factor that was later corrected by Rice [70]. The closed-crack case assumes a Coulomb friction law. As for the resistance function in the SCRAM model, the amount of energy tied as surface energy in a body weakened by penny-shaped cracks can be written as:

$$\psi^d = \gamma \sum_i \mathcal{N}_i s_i^c \tag{33}$$

where γ is the surface energy of the matrix and the expression for s_i^c, the area of a penny crack, is given in Eq. (8). The rate of change of this energy with respect to the crack-density parameter is the resistance, such that:

$$\mathcal{R}_i = \partial_{\mathcal{E}_i}\psi^d = \gamma\frac{4\pi}{3}\left(\frac{\mathcal{N}_i}{\mathcal{E}_i}\right)^{1/3} = \gamma\frac{4\pi}{3}\frac{1}{a_i} \tag{34}$$

The resulting physical interpretation is that cracks can only grow in the material if the rate at which potential energy is consumed matches the rate at which energy is tied in the form of new surfaces. This resistance function is analogous to the case of a flat R-curve from LEFM, since the energy necessary to create a unit area of crack is constant (and equal to γ), and, apart from SCRAM, is also used in the context of energy-based Micromechanical models by many authors [2,3,8,40,42,43]. Isotropic versions of SCRAM and other closely related formulations using this damage condition also exist [5,71–74], but are not discussed further.

Another example of a stress-based criteria derived from LEFM are two works by Iskhakov et al. [3,42]. These papers deal with damage induced by the expansive products of alkali-silica reactions in concrete, which is also the source of prior works on micromechanical modeling [1,2]. In Refs. [3,42], the authors assume that damage in the aggregates and the cement gel that compose the concrete can be modeled by the growth of pre-existing cracks using an energy-based criterion like the ones previously described. However, the authors also introduced another criterion where damage can form in a ring around aggregates and propagate through the gel. For that latter case, the damage loading condition is written as:

$$f_i^d = K_i^I - K^{Ic} \leq 0 \tag{35}$$

where K_i^I is the mode-I stress intensity factor (calculated for the case of an annular crack around the aggregate) and K^{Ic} the mode-I fracture toughness of the gel. No consideration is taken regarding mode-II fracture and compression, since the focus of the paper is on the behavior of chemically induced expansion (which is tensile and volumetric). In this case, K_i^I can be considered the driving force and K^{Ic} the damage-resistance. A similar fracture toughness approach is taken by Shao et al. [44,45], where a phenomenological modification is used to address compression. The stress-intensity factor for a crack i in an infinite elastic body for mode-I loading is typically presented as:

$$K_i^I = k_c\sqrt{a_i}\sigma^\infty \tag{36}$$

where σ^∞ is the remote stress, assumed to be a uniaxial tensile loading normal to the crack, and k_c is a constant factor which depends on the type of crack. Starting from this point, Shao et al. [44,45] proposed an equivalent stress to replace σ^∞, which has the form:

$$q_i^\sigma = \sigma_i^N\left(\frac{f_c}{f_c + \langle -\sigma_i^N\rangle}\right)^m + \alpha_a\left\langle 3\sigma_i^D\right\rangle \tag{37}$$

where σ_i^D is the normal component of the projection of the *deviatoric* stress tensor into the crack plane, as opposed to σ_i^N, which refers to the complete stress tensor. The exponent m is a free model parameter, with f_c being the compressive strength of the homogenized material, and α_a being a small factor that increases linearly with crack diameter until a critical diameter value, after which it is held constant.

Under uniaxial tensile loading aligned to the ith crack family, the model by Shao et al. [44,45] closely approximates the classical LEFM/fracture toughness approach. On the other hand, the compressive behavior is modeled phenomenologically. Notably, this model predicts that compressive damage will happen by propagating a crack whose normal direction is aligned with the compressive one. This is in stark contrast to the assumption of most other micromechanical models, which consider that compressive damage will trigger the growth of cracks either at an angle with respect to the compressive direction (such as in some works of Zhu and collaborators [16,17,19]) or of those whose normal vectors are perpendicular to the loading directions [2,43].

3.3. Strain-based evolution criteria

Rather than using the energy-release rate or components of the stress tensor to compose the driving force in their model, the formulation by Jefferson and Bennett [49,50], later extended by Mihai and Jefferson [75–78], writes this force in terms of components of the *strain* tensor exclusively. Conversely, their damage-resistance function is purely dependent on an auxiliary damage parameter ζ_i, which has the meaning of an equivalent damage strain. Under these assumptions, the damage-loading function takes the simple form:

$$f_i^d = f_i^d(\boldsymbol{E}, \zeta_i) = \mathcal{F}_i(\boldsymbol{E}) - \mathcal{R}_i(\zeta_i) \tag{38}$$

and was originally written as a strain-based version of the hyperbolic Mohr–Coulomb surfaces often used in cohesive element formulations for quasi-brittle materials. In this original form, the resistance function is simply $\mathcal{R}_i = \zeta_i$. The damage parameter ζ_i is then tied to the actual damage scalar, which acts to soften the effective stiffness tensor based on the MT estimate. The model uses the strain-based friction approach briefly mentioned in Section 2.3 and discussed in detail in Annex A. More details about Eq. (38) can be found in Annex B.

It must be noted that this model represents a certain departure from the others discussed in this section, in the sense that it can be considered, at least from the perspective of damage evolution, to be entirely phenomenological. Contrary to energy- and stress-based formulations, where principles of LEFM and/or thermodynamics are employed, this damage evolution law is not derivable from first principles. It can also be argued that using the *total* macrostrain tensor (or, more specifically, projections of it) is somewhat contradictory to the underlying assumption of the theory laid out in Section 2, where the contributions of each crack family are summed in strain space and the macrostress is shared by all families.

Another consequence of writing the damage evolution laws in terms of the macroscopic strain tensors is that the contributions of each crack family in terms of added strains/compliances have to be integrated numerically. If this is not done, damage evolution in the homogenized material becomes pathologically dependent on the directional discretization of the problem in terms of the number of crack families. This is due to the fact that changes in the damage state of one crack family do not affect the damage-loading functions of the others. As such, adding more families therefore increases the total amount of damage in the material, which must be compensated by the integration weights. In the paper by Jefferson and Bennett [50], a Maclaurin integration over a unit hemisphere is employed.

For energy- and stress-based models, changes in the damage state of one family do affect the damage-loading functions of all others, since increasing damage leads to a global reduction in stress or free energy, not only a local one. As such, the crack families are coupled, and the use of integration weights in these models is inappropriate, as it would also lead to nonobjective behavior with changing directional discretization. For these formulations, crack families should simply be distributed, rather than integrated, and for isotropic damage initiation this distribution should minimize directional sampling bias as much as possible.

3.4. Overview of models and equivalence between formulations

By combining the previously discussed choices for the type of damage evolution, friction formulation, and crack-closure approach, several different models can be obtained. Additionally, authors can also make assumptions on the nature of the distribution of crack families, with orthotropic and isotropic versions of both energy and stress-based formulations existing, as highlighted. A summary of these different modeling choices, and how different works fall into each category, is given in Table 3.

Remarkably, it can be shown that some of these formulations, while looking on the surface rather different, are in fact equivalent, at least in some constrained scenarios. To demonstrate this equivalence, no friction is considered, such that the energy expression in Eq. (28) can be used. In that case, an energy-based model using the MT estimate yields the following driving force, written for prescribed stresses:

$$\mathcal{F}_i = \frac{1}{2}\boldsymbol{\Sigma} : \mathbb{H}_i^{*|\circ} : \boldsymbol{\Sigma} \tag{39}$$

This expression is independent of the damage parameter, since the $\mathbb{H}_i^{*|\circ}$ tensor is constant and depends only on the direction of the crack family, not its characteristic size or the number of cracks per unit volume. For an isotropic matrix, this driving force yields the expression in the SCRAM model (Eq. (31)) exactly. This equivalence was also observed to hold for the case of frictional cracks (which was done numerically and not formalized here). While such an equivalence may seem surprising at first, it makes more sense once it is recalled that the MT estimate matches the compliance-based Dilute one for the case of penny-cracks. Since this Dilute estimate is directly obtained from the Eshelby tensor, without any assumption other than the infinite nature of the elastic medium with respect to the size of the crack, it must therefore be exact, since the Eshelby tensor is also defined exactly in the case of isotropic matrices and ellipsoidal inclusions.

Another equivalence that can be proven is between the stress-based models, namely the Griffith's approach of SCRAM, and those based on the stress-intensity factor, at least for the case of loading normal to the crack plane. This can be done by squaring the

Table 3
Classification of cited literature based on damage, friction, and crack closure mechanisms.

Type of mechanism	Modeling choices		Publications
Damage propagation	Anisotropic (N independent crack families)	Free energy-based	[11,12,15–17,41,47]
		Stress components-based	[6,44,45,48]
		Strain components-based	[49,50,75–78]
	Orthotropic (3 independent crack families)	Free energy-based	[2,3,42,43]
		Stress components-based	[3,42]
	Isotropic (single damage parameter)	Free energy-based	[4,19,21,51–60,62,66,67]
		Stress-based	[5,71–74]
Friction	Friction not considered		[2,3,12,15,16,41–43,66]
	Local	Plasticity-based	[11,17–19,47]
		Stress rate-based	[6,48]
		Strain-based	[49,50,75–78]
	Global	Plasticity-based	[4,21,51–60]
Crack closure	Considered by the choice of Dilute concentration tensor		[6,12,15,16,41,44,45,48]
	Considered by the local friction formulation		[11,17–19,47,49,50,75–78]
	Not considered/Considered globally only		[2–5,19,21,42,43,51–60,62,66,67,71–74]

two terms that compose the damage-loading function in Eq. (35). Since the limit surface itself is defined by $f_i^d = 0$, it remains the same under this squaring, even if the value of the damage-loading function changes elsewhere. The new (squared) damage loading function can be written, with some manipulation, as:

$$f_i^{dK} = \left(\sigma_i^N\right)^2 - \left(\frac{K^{Ic}}{k_c}\right)^2 \frac{1}{a_i} \tag{40}$$

where σ^N is the remote normal stress applied to the crack family (which, for penny cracks, is the same as the average stress in the matrix). The SCRAM function is now similarly rearranged as:

$$f_i^{d\gamma} = \left(\sigma_i^N\right)^2 - \frac{1}{k_e}\frac{4\pi\gamma}{3}\frac{1}{a_i} \quad ; \quad k_e = \frac{8(1-\nu)(1+\nu)}{3E} \tag{41}$$

where E in the Young's modulus. Comparing the two expressions, they have the same functional dependency on $\left(\sigma_i^N\right)^2$ and $1/a_i$, differing only by the format for the constant term multiplying the latter. Therefore, if the K^{Ic} parameter is written as:

$$K^{Ic} = \sqrt{\frac{k_c^2}{k_e}\frac{4\pi}{3}\gamma} \tag{42}$$

the two formulations are identical.

An important property of these equivalent formulations (henceforth referred to as the 'LEFM models') is that they require finite defects to be initially present in the material. Without initial defects, the damage-loading condition can never be reached, regardless of the magnitude of the applied strains/stresses. For the surface energy approach, this is because the resistance function becomes infinite for vanishing (initial) crack radius. In the fracture toughness approach, the driving force remains null.

Another aspect that must be highlighted is that these demonstrated equivalences only hold for the narrow cases described. If an energy-based model is used with a different estimate than MT, the surface energy resistance function does *not* yield the SCRAM stress-based expression. In fact, in those cases, the stress-based driving force of the former model remains a more complex function of the damage parameter whose functional dependency varies with the choice of homogenization scheme. The result is not constant as in Eq. (39), obtained for the MT estimate. Further, the surface energy approach is only the same as the fracture toughness one for mode-I loading. If shear is applied, this equivalence no longer holds. In fact, it is also possible to write stress-intensity models with mode-II and mode-III loading taken into account. These are hardly discussed in the context of analytical-based micromechanical models.

It is remarked that while the MT estimate was used by all the stress-based models cited, and the equivalence with the energy formulation only exists in this case, it is also possible to use stress-based damage-loading functions with other estimates. An example of this is given in Fig. 1 for uniaxial tensile loading, where a_0 is the initial radius assumed for all crack families.

4. A critical look at micromechanical models

The behavior of micromechanical models is directly tied to the interaction between the driving force $\mathcal{F}_i$, the resistance function $\mathcal{R}_i$, the choice of homogenization scheme, and the nature of the applied mechanical loading. These choices have profound consequences on the pre- and post-peak behavior of the models; the stability of the constitutive law and of the distribution of damage along multiple directions; the physical meaning of the formulation; and the capacity of the models to reproduce well-known experimental results; among other things. In this section, these choices are examined, along with some important issues that affect most micromechanical formulations currently available in the literature.

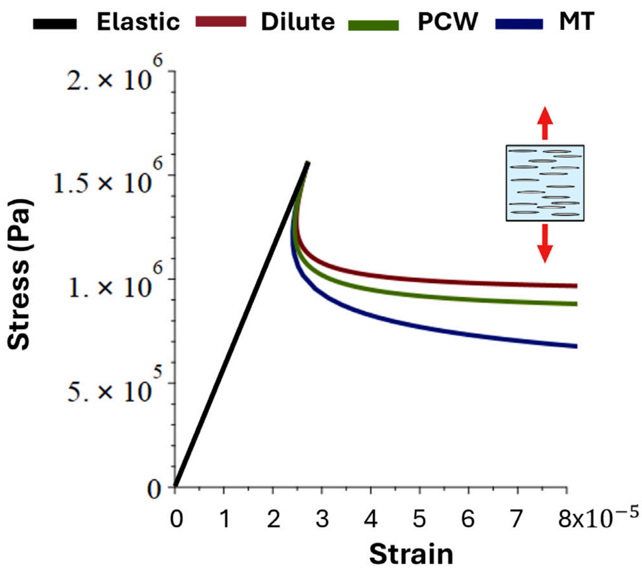

Fig. 1. Uniaxial tensile stress–strain response of an isotropic matrix (E = 60 GPa, ν = 0.2) weakened by a single family of penny-cracks whose normal axis is aligned with the loading direction. The damage-loading function is based on the fracture toughness approach in Eq. (35) with parameters a_0 = 0.02 m, $\mathcal{N}$ = 10^3 m^{-3}, K^{Ic} = $10^6/4$ Pa/$\sqrt{\text{m}}$. The Dilute, PCW, and MT estimates are used. In this figure, 'Elastic' refers to the portion of the stress–strain curves before the initially assigned damage starts to increase.

4.1. Accuracy of mean-field homogenization schemes

A central assumption in the micromechanical models discussed in this work is that mean-field homogenization theory can be used to estimate the effective behavior of the cracked medium. To validate this assumption, it is useful to compare the predictions of different homogenization schemes to those of FEM models. Such comparisons are numerous for plane stress cases, where the cracks are 1D lines (e.g. Refs. [22,79–82]). However, 3D studies with (2D) penny cracks, which are more relevant to this work, are also rarer. Two related papers by Bluthé, Bary, and Lemarchand [83,84] examine the effects of cracks placed in parallel with a random distribution on an isotropic matrix, such that the effective behavior is transversely isotropic. Vasylevskyi, Drach, and Tsukrov [85] do the same, but for a matrix that is initially orthotropic. Lastly, Saenger, Krüger, and Shapiro [86] consider both randomly oriented and randomly distributed cracks in an isotropic matrix. For higher density parameters, the cracks are allowed to intersect in the isotropic case, since forbidding the intersections becomes virtually impossible above a certain crack-density threshold. Further, contrary to the other references listed, the authors deal with wave-propagation speeds, rather than the (directly related) elastic constants. Nevertheless, the two measures will be considered as qualitatively equivalent for the purpose of this analysis.

Taking into account the aforementioned works, it can be generally noted that the Dilute [83] and PCW/IDD [79,82,83] homogenization schemes largely *under*estimate stiffness and display a percolation threshold (a complete loss of stiffness for finite crack densities). These results can be observed in Fig. 2, where the predictions from these schemes are compared to the FEM results reported by Bluthé, Bary, and Lemarchand [83] for the case of aligned cracks. It should be highlighted that since mean-field estimates neglect overlap between cracks, the existence of this threshold is inconsistent [22,23,87]. However, these estimates predict it under fairly low crack-density parameters. Conversely, the MT estimate [79–83,85,86], which does not display a percolation threshold, largely *over*estimates stiffness, as can also be seen in Fig. 2. In fact, as highlighted by several authors, the MT estimate represents an upper-bound prediction of the effective stiffness for a random distribution of non-intersecting cracks [36,88–90]. This is actually a general problem with the estimate, which tends to considerably under- or overestimate the effective elastic properties of the homogenized medium in situations of high contrast between the elastic properties of the matrix and the inclusions, the case of void inclusions being an extreme example.

From a physical perspective, a percolation threshold should not exist in the case of planar, randomly placed, aligned cracks — such as in Fig. 2. Aligned flat cracks would only lead to fragmentation if they become sufficiently large to bisect the entire bulk of the material, in which case it is no longer possible to define an RVE and analyze these cracks statistically (as done in micromechanical models). Therefore, the existence of a threshold in the Dilute and PCW/IDD estimates for the case of aligned cracks can be considered a mathematical artifact. In contrast, for randomly distributed cracks, overlap is essentially inevitable at sufficiently high density parameters, as highlighted in Ref. [86]. Here, a percolation threshold should indeed emerge once a sufficient number of cracks are connected. In this case, the MT estimate is inadequate, since this threshold is not present for finite density parameters. Indeed, while reaching this threshold again marks the limit of the RVE's validity, a representative model should nevertheless capture the transition point. By remaining finite, the MT estimate implies that the statistical procedure remains valid indefinitely, regardless of density.

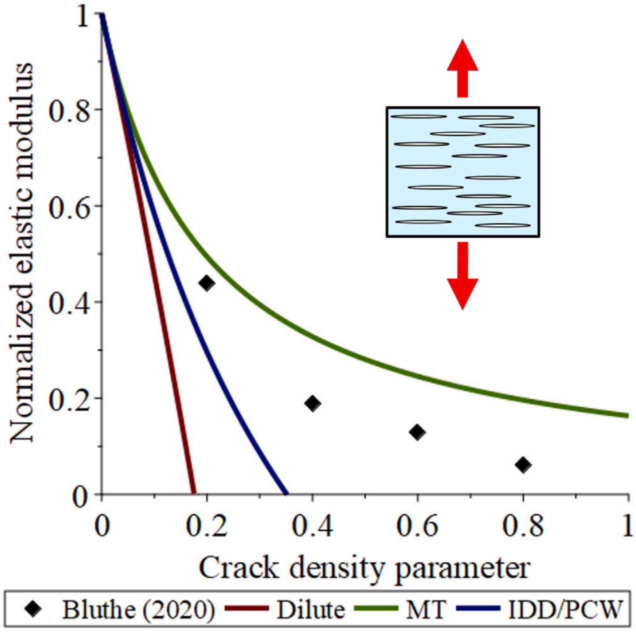

Fig. 2. Comparison of mean-field homogenization schemes and FEM results [83] in terms of normalized elastic modulus along the Z-axis. The results are obtained considering a single crack family with normal axis aligned with the Z-axis and embedded in an isotropic matrix ($\nu = 0.2$).

As for the IDD/PCW and Dilute estimates, even though a threshold is present, its value is arbitrary, insensitive to the distribution of crack directions, and generally too low.

Because of the complications introduced by the presence of percolation thresholds – especially if they are too low – researchers often prefer the MT estimate for numerical modeling purposes. This is also the case for the numerical examples presented later.

4.2. Stability analysis of energy and stress-based models

Numerically, damage evolution is normally imposed with a 'return' algorithm: once the damage loading condition is violated in a certain crack family ($f_i^d > 0$), the damage parameter $\mathcal{E}_i$ is increased by an amount that ensures $f_i^d = 0$ (to a certain tolerance). This implies the necessity that the damage-loading function decreases with increasing damage, otherwise a return to zero is not possible, since $d\mathcal{E}_i > 0$. Hence, the stability condition of micromechanical models can be written, in a general way, as $\partial_{\mathcal{E}_i} f_i^d < 0$. Assuming that that $\mathcal{R}_i$ is only a function of $\mathcal{E}_i$, which is typical, then yields:

$$\partial_{\mathcal{E}_i}\mathcal{F}_i - \mathcal{R}_i' < 0 \tag{43}$$

where $\mathcal{R}_i'$ is the derivative of the ith resistance function with respect to the ith damage parameter. This expression can then be used to analyze the stability of different formulations.

Starting with energy-based models, the driving force is fixed by the choice of homogenization scheme. Assuming no friction and prescribed strains, as in the simplified energy expression in Eq. (27), the stain form of the driving force in Eq. (29) can be written directly as:

$$\mathcal{F}_i = -\frac{1}{2}\boldsymbol{E} : \partial_{\mathcal{E}_i}\mathbb{C}^{*|\circ} : \boldsymbol{E} \tag{44}$$

Hence, the driving forces for the three select mean-field estimates can be obtained by differentiating their (frictionless) stiffness estimates with respect to the damage parameters. For the PCW estimate, this derivative can be written, with some algebraic manipulation, as:

$$\partial_{\mathcal{E}_i}\mathbb{C}^{*|\circ(PCW)} = -\mathbb{C}^m : \left(\mathbb{I} + \sum_j \mathcal{E}_j\mathbb{M}_j^{*|\circ} : \mathbb{S}^D\right)^{-1} : \mathbb{M}_i^{*|\circ} : \left(\mathbb{I} + \mathbb{S}^D : \sum_j \mathcal{E}_j\mathbb{M}_j^{*|\circ}\right)^{-1} \tag{45}$$

The MT and Dilute estimates can then be obtained, respectively, by assuming $\mathbb{S}^D = \mathbb{I}$ and $\mathbb{S}^D = \mathbb{O}$, as discussed in Section 2.1. Further, combining Eqs. (43) with (44) then yields:

$$-\frac{1}{2}\boldsymbol{E} : \partial^2_{\mathcal{E}_i\mathcal{E}_i}\mathbb{C}^{*|\circ} : \boldsymbol{E} - \mathcal{R}' \leq 0 \quad \text{or} \quad \frac{1}{2}\boldsymbol{E} : \partial^2_{\mathcal{E}_i\mathcal{E}_i}\mathbb{C}^{*|\circ} : \boldsymbol{E} + \mathcal{R}' > 0 \tag{46}$$

the latter of which is the stability condition given in Refs. [8,91].

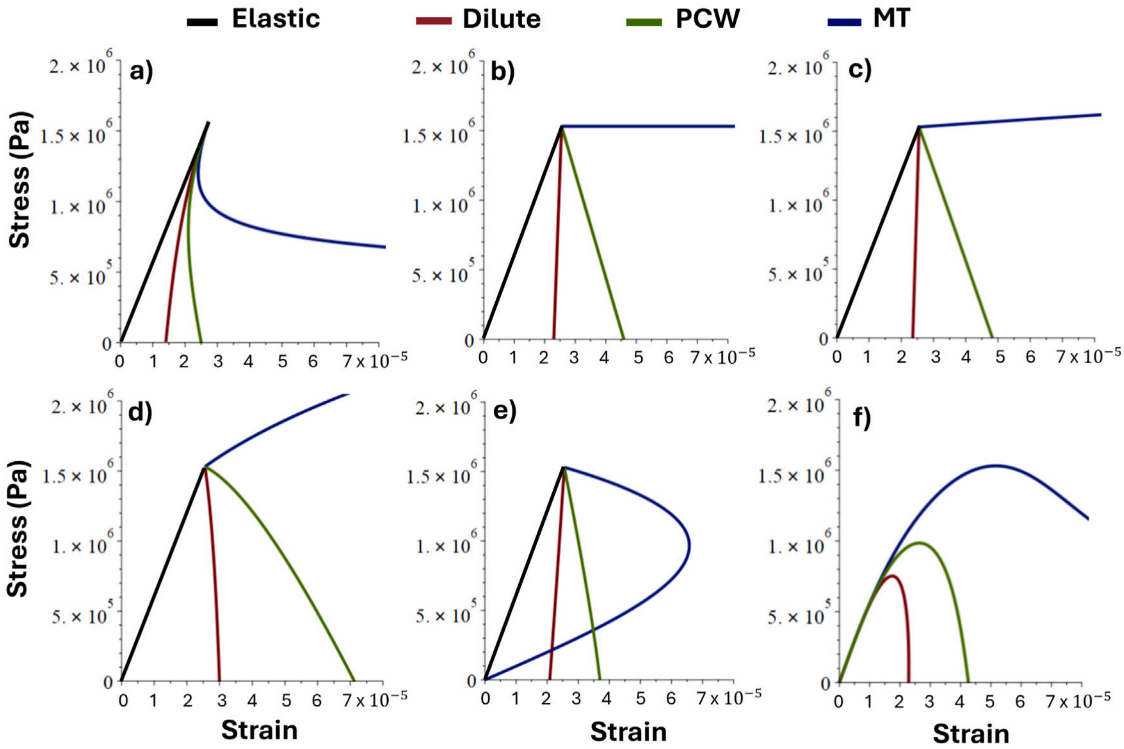

Fig. 3. Uniaxial tensile stress–strain response of an isotropic matrix ($E = 60$ GPa, $\nu = 0.2$) weakened by a single family of penny-cracks whose normal axis is aligned with the loading direction. The driving force is energy-based, while different resistance functions are considered, namely **(a)** the surface energy-based resistance function ($\gamma = 0.5\ \mathrm{J\,m^{-2}}$, $\mathcal{N} = 10^3\ \mathrm{m^{-3}}$, $a_0 = 2 \cdot 10^{-2}$ m); **(b)** the constant resistance function ($b_0 = 100\ \mathrm{J\,m^{-3}}$); **(c)** the linear resistance function ($b_0 = 100\ \mathrm{J\,m^{-3}}$) with slow hardening ($b_1 = 30\ \mathrm{J\,m^{-3}}$), **(d)** with fast hardening ($b_1 = 400\ \mathrm{J\,m^{-3}}$), **(e)** and softening ($b_1 = -100\ \mathrm{J\,m^{-3}}$); **(f)** and the hardening-softening resistance function ($r_c = 100\ \mathrm{J\,m^{-3}}$, $\mathcal{E}_c = 0.2$).

Imposing the stability condition in Eq. (46) based on the stiffness derivative in Eq. (45) (and the MT and Dilute variants of it), a few things are immediately clear. For all the estimates, the driving force of frictionless energy-based models is strictly non-increasing ($\partial_{\mathcal{E}_i}\mathcal{F}_i \leq 0$), and hence the stability condition is always satisfied for a 'hardening' resistance function ($\mathcal{R}_i' > 0$), meaning that all estimates are stable in this case (of fixed strains and increasing resistance to damage propagation). On the other hand, a decreasing (or constant) resistance function leads to an inherently *un*stable behavior for the Dilute estimate. This is because the stiffness derivative of this estimate is constant, and hence $\partial_{\mathcal{E}_i}\mathcal{F}_i^{(D)} = 0$, such that $\partial_{\mathcal{E}_i} f_i^d$ is positive, rather than negative — once the damage condition is violated, it can no longer be satisfied by increasing the damage parameter. For the other estimates, stability is ensured in 'softening' resistance functions only if $\mathcal{R}_i$ decreases more slowly than $\mathcal{F}_i$ (meaning that the first term in Eq. (46) is larger in magnitude than the second). This analysis is difficult to conduct for the MT and PCW approaches, since the second derivative of the stiffness tensor is more involved, and the stability condition will depend on the nature of the resistance function and of the prescribed strains. For the MT estimate in particular, the stability analysis is easier to conduct indirectly with the stress version of the driving force in Eq. (39). The implication of this format is rather curious: since the $\mathbb{H}_i^{*|\circ}$ tensor is constant, the resistance function dictates the behavior of the MT estimate very directly. To illustrate this, loading is assumed monotonic, such that $\boldsymbol{\Sigma} = \alpha\bar{\boldsymbol{\Sigma}}$, with $\bar{\boldsymbol{\Sigma}}$ being the (fixed) loading direction and α a scaling parameter. In this case, the damage-loading function is simplified as:

$$f_i^{d(MT)} = \alpha^2 C - \mathcal{R}_i \tag{47}$$

where C is a positive constant whose particular value is not relevant for this analysis. Forcing the damage condition $f_i^{d(MT)} = 0$ then yields:

$$\alpha^2 \propto \mathcal{R}_i \tag{48}$$

Hence, when $\mathcal{R}_i$ softens/hardens, so do the stresses (to a second power).

Many examples of the connection between the behavior of the resistance function and that of the stress–strain curves in the MT estimate can be seen in the literature. In Refs. [64,92], a softening resistance function leads to constitutive-level snap-back in the MT estimate for some parameter combinations, which then reverts back to stable softening. This snap-back instability is triggered when the stress-softening imposed by the condition in Eq. (48) is too fast. In that case, the constitutive equation $\boldsymbol{\Sigma} = \mathbb{C}^{*|\circ} : \boldsymbol{E}$ can only be satisfied by reducing the magnitude of the strains (and hence the snap-back). In Refs. [8,18,35,66], a constant $\mathcal{R}_i$ leads to a behavior that is akin to a perfectly-plastic response, but with secant unloading to the origin. Lastly, in Refs. [18,51], a hardening resistance function leads to hardening stresses — even under growing damage parameters. As discussed before in this section, these latter two cases (of non-decreasing resistance functions) are strictly stable under fixed strains. All of these behaviors can also be observed in Fig. 3.**(a)–(c)**, which will be discussed in more detail later.

A similar stress-based analysis can be conducted for the dilute estimate. In this case, the stress-based driving force is:

$$f_i^{d(D)} = \frac{1}{2}\boldsymbol{\Sigma} : \left(\mathbb{I} - \sum_j \mathcal{E}_j \mathbb{M}_j^{*|\circ}\right)^{-1} : \mathbb{H}_i^{*|\circ} : \left(\mathbb{I} - \sum_j \mathcal{E}_j \mathbb{M}_j^{*|\circ}\right)^{-1} : \boldsymbol{\Sigma} - \mathcal{R}_i \tag{49}$$

It can be noted that the driving force part of this expression increases with increasing damage and does so particularly rapidly around the percolation threshold. This rapid increase means that the damage evolution condition can only be satisfied by either a rapidly increasing resistance function or by rapidly decreasing stresses. In the latter case, snap-backs can also occur if the stress reduction is too quick. Several instance of this behavior can also be observed in Fig. 3. A similar rationale is also valid for the PCW estimate. However, the derivative in this case is more involved and will not be discussed here.

For the LEFM-based models, such as those using surface energy and fracture toughness resistance functions, an important stability consideration is that small initial defects can lead to constitutive-level snap back, especially when the number of defects per unit volume is also small. Some examples of this can be seen in Fig. 3.**(a)**, where a small number of small defects induces brittle failure in both the Dilute and PCW estimates, along with constitutive level snap-back in the initial part of the softening curve of the MT estimate. In the latter case, another problem can also be observed: both the fracture toughness and surface energy approaches lead to stress–strain curves that do not fully soften for finite density parameters. While Fig. 3 was generated exclusively with energy-based models, the same problems also occur with the stress-based formulations, even when estimates other than MT are used, such that they are no longer strictly equivalent to the energy-based MT model, as described in Section 3.4. This can be seen in the previous figure (Fig. 1), where a toughness-based resistance function leads to snap-back in the initial parts of the softening curve for all estimates, which then reverts back to stable softening that flattens out at overly large stresses.

Here, it is important to highlight how the inelastic parts of the plots in Fig. 3 are created. These results are obtained from the stress version of the energy damage-condition (and hence represent the damage-condition under fixed *stresses*, not strains). The damage condition is then forced ($f_i^d = 0$), from where the stress magnitude (under a uniaxial tensile-load) that satisfies this condition is obtained as a function of the crack-density parameter. The strains associated with this stress/crack-density pair are obtained by multiplying the stress itself by the density-dependent compliance. Under these conditions, it is possible to trace the stress–strain curve using the density-parameter as a parametric variable. An analogous process was also used to compose Fig. 1, which uses the stresses directly, rather than through an energy-based formulation.

Another key point is that in both the Dilute and PCW cases, damage evolution is interrupted before the percolation threshold. If damage is allowed to increased until percolation, both estimates snap-back towards the origin sharply until complete loss of cohesion. After this point, damage cannot be allowed to increase, otherwise the model response becomes non-physical.

Lastly, the stability condition of the strain-based formulation of Jefferson and Bennett is trivial. Since the driving forces in Eq. (69) is dependent only on the strains, and the resistance functions are the auxiliary damage parameters ζ_i themselves, the derivative of f_i^d in Eq. (38) with respect to ζ_i is negative and unitary. Hence, the damage problem is stable. As for instabilities in the stress–strain curve, snapbacks in tension can be easily prevented by a careful choice of functional dependency connecting the auxiliary damage parameters to the actual damage variables. In compression, however, the presence of friction can sometimes trigger unstable softening, which is difficult to formally analyze.

4.3. Choice of damage-loading function

For energy-based models, the driving force is fixed by the choice of homogenization scheme, and hence only the resistance function can be chosen somewhat freely. Still, this resistance expression must be consistent with the meaning of the driving force — namely, it has to represent the rate of energy expenditure necessary to increase material damage. In stress and strain models, on the other hand, the choice of both the resistance function *and* the driving force is less constrained. Hence, many more options are available for composing the damage-loading function. However, regardless of the type of model, the damage-loading functions of micromechanical models are essentially of 3 kinds:

- Physics-based, which are often derived from principles of LEFM and can be tied to well-known physical laws;
- Phenomenological, where the functional form is not derived from any clear laws or principles, but rather proposed as a way of matching experimental data for a given driving force and homogenization scheme;
- Semi-phenomenological, where principles of LEFM are used to obtain some aspect of the functional form, with modifications to capture more complex phenomena that cannot be readily interpreted in a direct physical way.

Examples of formulations that are entirely or partially physics-based include the fracture toughness approaches of Iskhakov et al. [3,42] and of Shao et al. [44,45], and the equivalent surface energy approach of SCRAM [5,6] and of several energy-based models [2,3,8,40,42,43]. However, many entirely phenomenological formats for the damage-resistance function also exist in literature, particularly for energy-based models. A commonly used one [9,12,15–18,41] is to assume that it increases linearly with the crack-density parameter, such that:

$$\mathcal{R}_i = b_0 + b_1 \mathcal{E}_i \tag{50}$$

where b_0 and b_1 are (positive) constants that need to be fitted. As with other resistance functions, the behavior of this linear expression varies drastically depending on the choice of homogenization scheme. This can be seen in Fig. 3.**(c)**-**(d)** for different values of b_1 and the three chosen estimates. As shown in the previous section, a hardening resistance function automatically implies stress-hardening in the case of the MT estimate. Because of this forced hardening, such a combination is only used to fit experimental data where softening is not observed [17,41]. Alternatively, when paired with the PCW estimate [16], softening does happen and appears to be generally stable. This can also be seen in Zhu et al. [51] for a different (nonlinear) hardening function. As for the Dilute estimate, the stability of the uniaxial behavior seems to depend on the magnitude of b_1, with smaller values leading to snapback and larger values leading to stable softening. This is in contrast with the behavior under fixed strains, which was proven in the previous section to always be stable for increasing resistance functions. For this and all other PCW and Dilute examples, the softening curves are limited to density parameters below percolation. If percolation is reached, the behavior is always a sharp snap-back to the origin.

Some criticisms can be levied against the linear expression. The first one is that it lacks a clear physical meaning, since the b parameters are arbitrary model constants that are determined by back-fitting of experimental data. Further, a rising resistance function is more meaningful in the context of the R-curve from LEFM, where it increases with growing crack *extension*, *not* crack density. This increase is generally assumed to happen due to the formation of growing plastic zones around extending cracks. It is also assumed to reach a limit, such that the R-curve does not increase unboundedly. Hence, the motivation for an always-rising resistance function $\mathcal{R}_i$ in terms of the crack density parameter is less clear. Lastly, as shown in the previous paragraph, this format has drastically different behaviors depending on the choice of homogenization scheme and the magnitude of the b parameter. This can be problematic, as fits for one particular estimate cannot be generalized to others and might only be applicable to specific load cases.

Assuming $b_1 = 0$ reduces the linear format to a constant resistance function, which is also widely used [1,8,16,18,35,66]. Again, this format leads to different output depending on the selection of the homogenization scheme (Fig. 3.**(b)**). If the MT estimate is used, a response akin to perfect plasticity (with elastic unloading to the origin) is observed, as noted by several researchers. This can also be proven directly from Eq. (48), which can only be satisfied for a constant resistance function if the stress-magnitude scalar is also constant. If the Dilute scheme is chosen, it leads to constitutive-level snapback (as also previously discussed).

Still in the linear format, Fig. 3.**(e)** shows that negative values of b_1 again produce constitutive-level snap-back for both the Dilute and the MT estimate. In the former case, as in the previous sub-figures, this brittleness is inherent to the estimate itself — as discussed previously. As for the MT estimate, the snapback behavior at higher crack densities is caused by the value of the resistance function approaching zero when $\mathcal{E} = b_0/|b_1|$. When that happens, no finite driving force can satisfy the damage-condition. Since the driving force for energy-based models remains finite under any (also finite) value of the damage-parameter in the MT estimate, the damage-condition can only be satisfied if the strain is also decreasing. In fact, at a certain point, they decrease as fast as possible (as fast as a purely-elastic unloading, since there is no longer any energy being dissipated by the growing crack). Hence, the result in Fig. 3.**(e)**. Obviously, a null resistance to damage propagation under finite crack sizes is non-physical. Therefore, this format is added here only for illustrative purposes and is not used by any researchers (as far as the authors of this work are aware). It is also noted that this format leads to stable softening for the PCW and Dilute estimates only because of the chosen value of the b constants, which cause $\mathcal{R}$ to be zero when $\mathcal{E} = 1$ - above the percolation threshold of the estimates. If the $b_0/|b_1|$ fraction leads to a density parameter below this percolation threshold, snapback is also observed.

The clear connection between the stress–strain behavior of the MT estimate and that of the resistance curve allows authors to fine-tune the latter to match experimentally observed results in the former. To capture the transition from hardening to softening behavior of quasi-brittle material under uniaxial compression, Zhu and Shao [47] used the MT estimate together with the following hardening-softening resistance function:

$$\mathcal{R}_i = r_c \frac{2k_i}{1+k_i^2} \quad ; \quad k_i = \frac{\mathcal{E}_i}{\mathcal{E}_c} \tag{51}$$

where r_c is the critical value of $\mathcal{R}$, which is obtained when the crack-density parameter reaches its critical value $\mathcal{E}_c$, after which the material softens. Hardening-softening curves of this kind, or slight variations/generalizations of it, have been used in many papers [7,11,47,53,55–59,64,92]. However, the use of these functions may also lead to undesirable behavior of the effective material. For values of $\mathcal{E}_i/\mathcal{E}_c \ll 1$, the resistance function can be approximated as $\mathcal{R}_i \approx 2r_c\mathcal{E}_i/\mathcal{E}_c$. This implies that, for crack density parameters much less than the critical value $\mathcal{E}_c$, the resistance function is (roughly) linearly dependent on the crack-density parameter $\mathcal{E}_i$ *without* any constant term. Hence, at vanishing crack densities, this resistance function predicts the growth of cracks with also vanishingly low stresses, which has no physical basis. These low densities will give the appearance of a linear-elastic behavior, but this is not the case. In fact, the model has no elastic range — when $\mathcal{E}_i$ is no longer small, deviations from linearity become visible, which can be observed in Fig. 3.**(f)**. Further, the critical crack-density parameter $\mathcal{E}_c$ is often assumed by authors to be way beyond unity [47,56,57,59] in order to fit experimental stress–strain curves. As discussed in Section 4.1, such high values are far beyond the range where the MT estimate is reasonable. In fact, out of the MT plots in Fig. 3, the end-points in sub-figures **b**–**d** and **f** correspond to a crack density of 1, with the final crack-density in **a** being 2. These values are also beyond the range where the MT estimate can be considered reasonably accurate, despite the fact that the softening curve in Fig. 3**a** still presents a significant residual strength. This high residual strength is a direct consequence of the stiffness overestimation in the MT estimate and lowering its value would push the estimate further beyond its meaningful range.

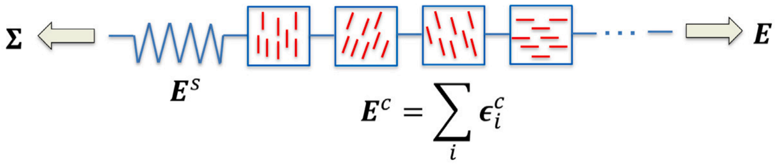

Fig. 4. Schematic representation of mean-field estimates for cracked media: the crack families are assumed to be connected in series and to be under the same (macro)stress. $\boldsymbol{E}^s = \mathbb{D}^m : \boldsymbol{\Sigma}$ is the strain contribution from the undamaged matrix, such that the total strain is $\boldsymbol{E} = \boldsymbol{E}^s + \boldsymbol{E}^c$.

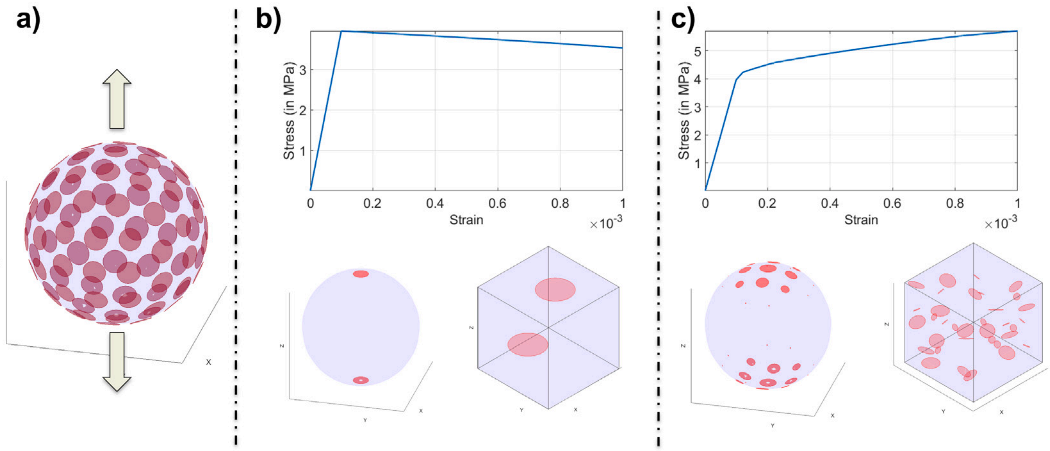

Fig. 5. (a) Illustration of the initial distribution of cracks, which are spread in an angular discretization over a hemisphere (mirrored for visualization purposes). The example is provided for the following parameters: an initially undamaged ($\mathcal{E}_0 = 0$) material with elastic constants $E = 40$GPa, $\nu = 0.22$; an energy-based damage evolution criterion; and 13 discretized directions. The sizes of the disks over the hemisphere surface reflect the relative (not absolute) values of the crack-density parameters in one crack family with respect to the others. This initial crack distribution is loaded in tension. **(b)** Stress–strain curves and final damage states for a linear resistance function in the softening case ($b_0 = 10^3 \mathrm{J\,m^{-3}}$ and $b_1 = -10^2 \mathrm{J\,m^{-3}}$). **(c)** Stress–strain curves and final damage states for the case of the linear resistance function with hardening ($b_1 = 5 \cdot 10^3 \mathrm{J\,m^{-3}}$). The cube visualization represents the absolute sizes of the crack inside the cubic REV, which are scaled down by a fixed factor for visualization purposes. For the examples in this work, the factor is 5.

4.4. Spurious direction localization

An inherent assumption of the mean-field homogenization models used in this work is that each crack family is under the same effective stress, which, in the case of penny cracks, is also the macroscopic stress. For the MT estimate, where each crack-strain contribution is linear with respect to this stress, each crack family can be essentially schematized as being connected in series, as illustrated in Fig. 4. This serial coupling has profound consequences for both stress-based models and energy-based models using the MT estimate.

Assuming no friction and proportional loading, if the increase in damage in a crack family leads to a reduction in the magnitude of the macroscopic stress, this causes the value of the damage-loading function in every other crack to decrease as well — hence, while the material is softening due to one crack family, the damage condition will never be reached in any of the other crack families in a (direction-)discretization of the cracking process. Essentially, this means that damage will localize into a single crack family: the one that starts to damage first.

Fig. 5 shows the crack propagation under uniaxial tension for different damage-resistance functions. Under uniaxial tension, damage localization will commonly happen in the crack family whose normal direction more closely aligns with the loading direction (5b). On the other hand, when the combination of driving force and damage-resistance is such that stress-hardening (rather than softening) happens, other cracks progressively reach the damage condition, with cracks whose normal direction is more closely aligned with the loading direction doing so first (Fig. 5c). The spectra of damage distribution in this case will depend on the final strain applied in the uniaxial loading and the magnitude of the hardening. An analogous example can be seen in Ref. [16], where the authors show that a linear resistance function with an energy-based driving force causes localization into a single crack family when $b_1 = 0$, but on multiple families when $b_1 > 0$. Further, the magnitude of b_1 is strongly correlated with the spread of damage: larger values lead to wider damage distributions, as also highlighted in this paper.

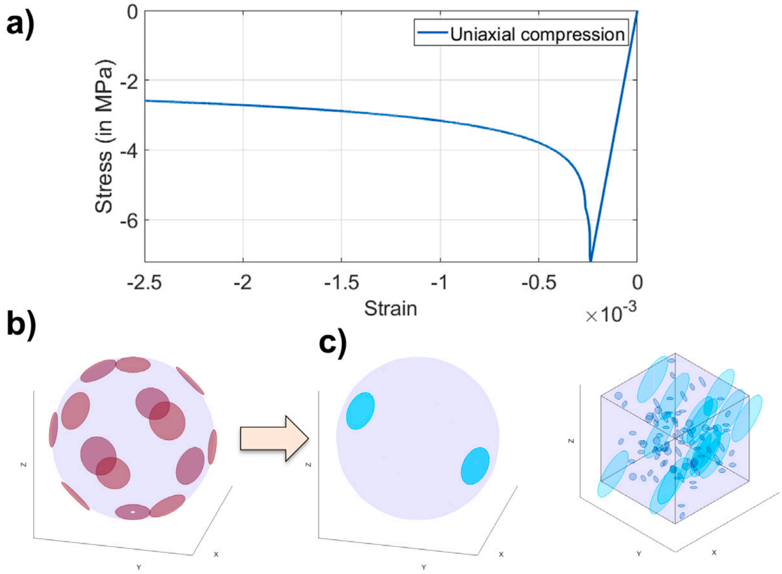

Fig. 6. **(a)** Stress–strain curve of a cracked material under uniaxial compression. **(b)** Initial distribution of cracks in the sphere representation. Red is used for open cracks (or, in this case, unloaded cracks), while light blue represents sliding and growing cracks. **(c)** Final distribution of cracks after localization. The sphere and cube representations carry the same meaning as in Fig. 5. Dark blue disks represent closed cracks that are not growing. The surface energy resistance function is used with material inputs $\gamma = 0.348$ J m^{-2}, $a_0 = 1.762 \cdot 10^{-3}$ m, $\mathcal{N} = 7.5 \cdot 10^7$ m^{-3}, $E = 40$ GPa, $\nu = 0.2$. The driving force is energy-based and 7 discretized directions are used in this example.

While tension offers a good illustration of the phenomenon, its main problem is more apparent when the material is under uniaxial compression, for which damage localization is an unstable process. An example of compressive damage localizing unstably into a single crack family (mirrored due to symmetry) can be seen in Fig. 6. The instability under compression can be understood as follows: if closure is considered, the cracks that reach the damage condition first are the ones that are at a certain angle with respect to the compression direction [71]. In the case of hardening, this damage spreads from the initial direction to other crack families that are similarly aligned. On the other hand, if the material softens, damage will remain concentrated where it started, just as in tension. However, since this crack family will be at an angle with respect to the loading direction, damage is asymmetric, contrary to tension. That leads to a highly unstable behavior where the direction of crack propagation can change drastically due to small perturbations in lateral stresses. This instability is exacerbated when the number of crack families is larger, such that the critical condition for crack propagation can be reached simultaneously on multiple cracks when the prescribed strain increments are larger.

The localizing behavior of softening energy-based models is briefly noted by Zhu, Yuan, and Shao [11] for the case of confined compression, where the process seems to be less unstable than what is described here. While this possibility is not investigated further, some preliminary numerical analysis by the authors of this work indicates that confinement indeed acts as a localization stabilizer, at least in the initial parts of the softening curve. However, localization still happens, and can still be highly unstable.

A notable exception to the localization behavior is the formulation by Jefferson and Bennett. In their model, the macroscopic strains are projected onto the individual crack planes to drive damage evolution. By evaluating damage based on this total macrostrain projection (rather than the macroscopic stress), the model effectively applies a kinematic assumption across all crack families for the purpose of damage evolution (in other words, parallel coupling). This fundamentally differs from the static equivalence assumed by the energy- and stress-based approaches (represented in Fig. 4 as a series coupling), where all crack families experience the same macroscopic stress. Because of this kinematic assumption, the discussed stress-relief mechanism responsible for unloading secondary cracks is absent. In turn, this allows damage to progress simultaneously across multiple crack orientations even under stress softening.

Examples of the lack of direction localization in the model of Jefferson and Bennett are given in Fig. 7 for both tension and compression. This figure also illustrates two particular features of the formulation: (i) damage evolution can happen even on locked cracks, which is not the case for the energy and stress-based approaches with local friction discussed in this paper, and (ii) cracks can be sliding even under tension, since contact is considered between the asperities of the crack surfaces. An important limitation of micromechanical models can also be noted in Fig. 7: while a non-interacting approach is used, it can be seen from the final crack distribution of the tensile example (Fig. 7a) that the crack-density parameter is exceedingly large, such that interactions between the cracks can no longer be neglected. In this case, the final crack density largely exceeds unity in several crack families, which is considerably beyond the values assumed reasonable for mean-field estimates in Section 4.1. This is again a consequence of the stiffness overestimation of the MT method.

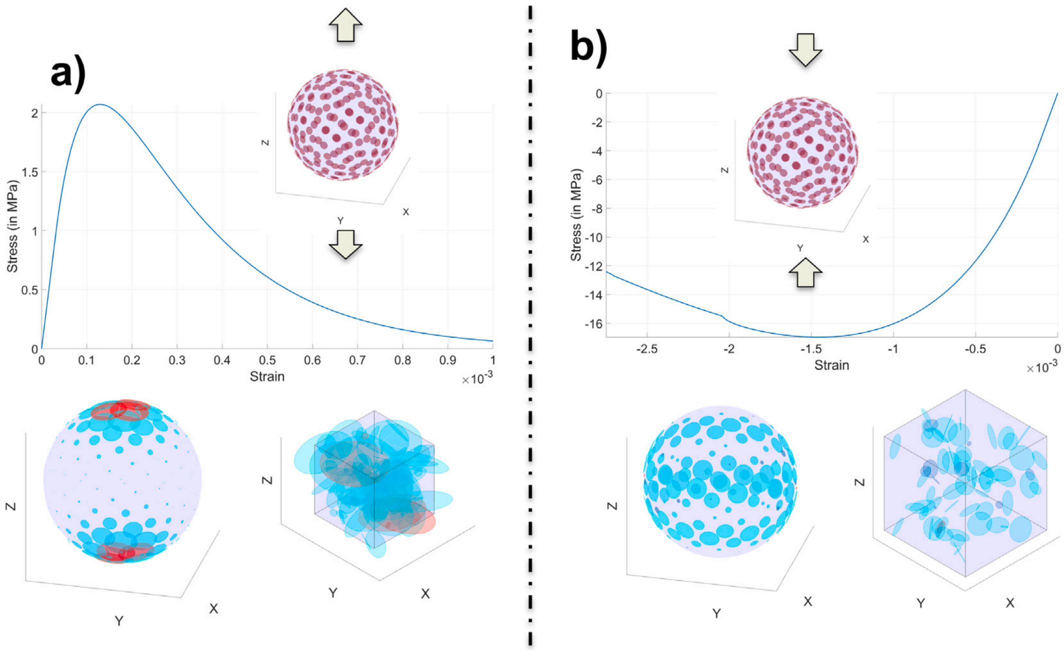

Fig. 7. Behavior of the strain-based model of Jefferson and Bennett under **(a)** uniaxial tension and **(b)** uniaxial compression. 100 crack families are initially used, which are represented on top of the stress–strain plots. At the bottom, the final damage distribution is illustrated in both the sphere and cube representations (which carry the same meaning as in Fig. 5). The model parameters are $f_t = 1$ MPa, $f_s = 1.5$ MPa, $\epsilon_{tu} = 10^{-3}$, $m_g = 0.2$. The meaning of these parameters can be found in Annexes A.3 and B.

It is noted that, in all the examples shown in this section, the problem is solved incrementally and implicitly for a single material point. For the energy-based models in Figs. 5 and 6, friction is neglected. As such, the simplified energy expression in Eq. (27) is used alongside the MT estimate in Table 2. This estimate is then generalized to allow crack closure using the modified $\overline{\mathbb{T}}_i^{*|\circ}$ tensors in Eq. (12). The LCP in Eq. (22) is solved by the Newton method. A staggered approach is used: for each damage increment in the Newton solver, the effective behavior is recalculated iteratively to ensure convergence of the opening/closure criterion for the frictionless cracks for the given strain and damage state. For the localizing examples, care is taken to ensure only one crack family reaches the damage condition in order to avoid spurious solutions. For the strain-based model of Jefferson and Bennett, the solution procedure for a given strain is fully explicit. Hence, implicit iterations are only required to ensure zero stresses in all stress components other than the one corresponding to the prescribed strain.

4.5. Tensile-compressive asymmetry

It is known that quasi-brittle materials have a significantly different behavior under tensile and compressive loading, here referred to as tensile-compressive asymmetry. Such an effect is difficult to capture correctly in micromechanical models. For instance, if crack closure and frictional sliding are excluded, micromechanical models with energy-based crack growth criteria produce limit surfaces where there is no asymmetry. This is because the quadratic form of the energy expressions is insensitive to the sign of the stress/strain components.

When crack closure is considered, some features of the tensile-compressive asymmetry arise, since negative normal components no longer factor into the calculation of the dissipated energy for each crack family. For most models with multiple independent crack families, uniaxial compression then triggers damage due to the sliding of cracks diagonal to the loading direction. In this case, however, the ratio between tensile and compressive strength is fixed — in fact, it is directly caused by the ratio between the tensile and the *shear* strength of the cracks. This is also not enough, since different quasi-brittle materials have different tensile-shear-compressive strength ratios. In particular, compressive strength values tend to be significantly higher than tensile and shear strength values.

Another approach is the model by Shao et al. [44,45]. In this work, compressive failure is directly considered by the normal component on the crack plane, and the cracks whose normal vector is aligned with the compressive direction are the ones that grow. As such, compressive damage at the material level is essentially imposed at the crack level directly (and phenomenologically). This is not the expected behavior, where the cracks that grow under compression are at an angle with the compressive direction which maximizes effective shear.

Experimental evidence indicates that the compressive loading of quasi-brittle materials frequently leads to failure due to splitting perpendicular to the loading direction. To achieve this result, Esposito and Hendriks [2] work with a series of assumptions that are very particular of their model. First, only the positive part of the strain tensor is used in the driving force calculation (which is inspired by Mazars [65]). This makes it so that cracks whose planes are perpendicular to the (compressive) loading direction have no contribution to the driving force and hence do not propagate — even though the formulation has no crack closure. Further, the model assumes that cracks have non-vanishing aspect ratios when they are considered in the calculation of the effective stiffness tensor. This finite ratio then introduces a void-fraction component to the stiffness tensor, such that even cracks whose normal vectors are orthogonal to the compression direction would reduce observed stiffness. Lastly, the authors of Ref. [2] consider three orthogonal crack families, along with loading that is volumetric and expansive in nature and/or uniaxial and aligned with one of the crack families. Under these assumptions, tensile loading affects the crack family whose normal direction is aligned with the loading direction, while compression affects the other two crack families. As such, tensile/compressive asymmetry can be imposed by controlling the (non-zero) thickness assumed for the cracks. This non-zero thickness also allows the model to achieve full softening, which, as previously demonstrated, is impossible with the combination of the surface energy resistance function and the MT estimate used in Ref. [2].

The approach of using three orthogonal crack families is also used by Refs. [3,42,43]. Refs. [3,42], however, do not deal with compressive loads. In fact, damage evolution in the three crack families is assumed to be the same. While this approximation is considered sufficient in the context of their work, where loading is volumetric and tensile in nature, the same cannot be said for other loading conditions, limiting the general applicability of the model. As for the model in Ref. [43], similarly to Esposito and Hendriks [2], only axial loads aligned with the crack families are addressed. In this case, the approach of having three orthogonal crack families with finite thickness is more appropriate. However, shear and/or multiaxial loads are likely to trigger the localization problem previously described in Section 4.4. Further, the behavior of the model in these cases will be strongly anisotropic.

Given the aforementioned limitations, the most popular solution to simulate the tensile-compressive asymmetric behavior is to introduce local friction in the models.[2] As previously discussed, this frictional component can be either based on stresses [5,6,17,18] or strains [49,50] (see Section 2.3 for an overview or Annex A for more details). However, local friction also causes other problems to the solution of the damaging process. In the stress-based frictional models, local friction prevents complete compressive softening from happening, even at very large strains. Further, it also leads to some instabilities, where previously-locked cracks slide very suddenly, causing sharp drops in the softening curve. Examples of this can be seen in some confined-compressive curves in Ref. [47] for the case of energy-based models, and were also observed under uniaxial compression for the strain-based formulation by the authors of this work. Further, the strain-based model is also known to suffer from contact chatter [76]. This can be observed by the small oscillation in the post-peak behavior of the compressive part of Fig. 7. For coarser discretizations, this behavior is more pronounced (as is the case in Ref. [76]).

Lastly, another issue that also has to be mentioned with regards to the tensile-compressive asymmetry of quasi-brittle materials is that tensile and compressive curves not only have different peak stresses, but also different shapes. In particular, compressive curves are often assumed to have pre-peak stress hardening and an overall more ‘rounded’ behavior around the peak. Tensile curves, on the contrary, tend to be linear up to near peak stresses and have more pronounced softening immediately after this peak stress is reached. However, in almost all energy-based Micromechanical models, the shapes of inelastic curves are largely imposed by the combination of the homogenization scheme and choice of resistance function. Hence, optimizing this combination to match the shape of one softening curve does not guarantee that the other is correctly represented. Examples include Fig. 6, where the surface energy resistance function leads to a compressive softening behavior that would be more appropriate for tension, rather than compressive loading, and the hardening-softening function in Fig. 3.**(f)**, where the opposite is true.

4.6. Non-homothetic crack growth

A key assumption of the models discussed so far is that growing cracks remain circular and planar. While small deviations from circularity generally have minor consequences [23] and tend to vanish under Mode-I growth [93], the assumption of planar evolution is much more problematic for other cases [94–103].

Non-planar growth occurs essentially anytime the applied loading is not normal to the initially planar crack. This misalignment introduces an asymmetry, causing the crack to extend out-of-plane starting from a particular point along its perimeter. As the crack grows, it minimizes Mode-II loading because energy is more efficiently dissipated in Mode-I, which has a much lower fracture toughness. Consequently, the critical corner extends out-of-plane to “search” for the loading direction that maximizes hoop stress.

As an example, inclined cracks under uniaxial tension grow such that their extending portions tend to align perpendicularly to the load [97]. Conversely, under inclined compression, out-of-plane “wings” form and tend to align parallel to the loading direction [98–103], as illustrated in Fig. 8. Analogously, pure shear stress on the crack plane drives propagation at an angle that maximizes hoop stress [96].

Modeling these non-planar trajectories significantly complicates the calculation of crack-strains, tractions, stress-intensity factors, and the rate of surface-area generation. Because exact trajectories typically require numerical methods, several authors [104–109] have proposed approximate schemes that replace out-of-plane curved cracks with equivalent flat cracks using modified angles, aspect ratios, or strain contributions. However, these models are generally limited to small deviations from flat geometries, single or few crack families, uniaxial or biaxial loading, and 2D plane stress conditions (slits) rather than 3D penny-shaped cracks.

[2] Jefferson and Bennett’s model also introduce asymmetry directly by virtue of the (signed) normal strain parameter in the driving force in Eq. (69).

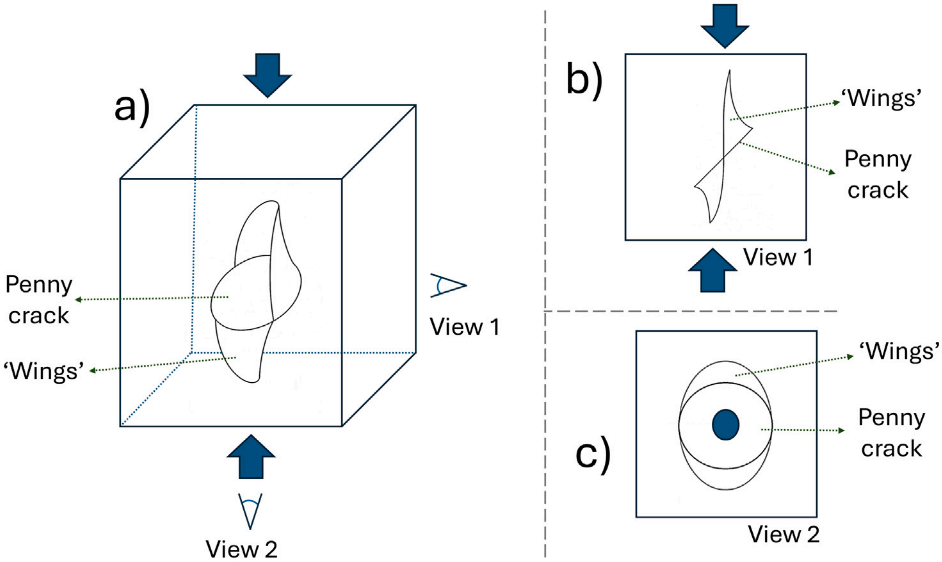

Fig. 8. Schematic representation of a winged crack. The crack starts as flat, planar, and circular (penny-shaped crack). Due to the presence of shear along the plane of the penny-shaped crack (such as when a uniaxial compression is applied perpendicular to the plane), it extends out of the plane in a manner similar to 'wings'. For a compressive load, the 'wings' tend to align with the compressive direction. **(a)** 3D view of the winged crack. **(b)** and **(c)** side-views, respectively perpendicular and parallel to the uniaxial compressive loading.

5. Conclusions

Micromechanical models are regarded as great alternatives to phenomenological formulations, especially for multiphysics and/or multiscale problems. This attractiveness comes from the fact that model input and internal variables are supposed to have clear physical meanings, such that coupling with non-displacement fields and across multiple scales is more intuitive. Further, these models appear to give very natural solutions to complex problems, such as anisotropic damage evolution and unilateral effects. However, these advantages are only fully realized if these models can correctly predict quasi-brittle behavior while maintaining a strong physical meaning. Upon a critical analysis of various approaches available in the literature, this paper highlights the following drawbacks of current micromechanical models:

- These approaches often adopt damage parameter values that are beyond the range of applicability imposed by the selected homogenization scheme.
- They can only capture specific loading cases under specific conditions, without being able to provide the correct softening behavior for general cases.
- Various models predict inelastic curves that are vastly different between different homogenization approaches, even within the range where they should all be valid.
- They rely on the assumption that cracks are planar, circular, non-percolating, and non-overlapping. For cases where damage evolution is allowed, particularly in the post-peak regime, these assumptions become increasingly non-representative the larger the damage.
- In case complex microstructures or failure mechanisms are considered, the nature of input and internal parameters generally tends to become phenomenological, or their values are beyond applicability ranges.
- Many models suffer from spurious localization of damage into a single crack family, which renders their behavior unstable.
- Local friction further adds instability to the model in the form of sudden crack sliding and contact chatter.

These findings seem to indicate that micromechanical models still require development to be suitable for broader applicability.

CRediT authorship contribution statement

Pedro Henrique Rios Silveira: Writing – original draft, Visualization, Validation, Software, Investigation, Formal analysis, Conceptualization. **Rita Esposito:** Writing – review & editing, Supervision, Project administration, Methodology.

Declaration of competing interest

The authors declare that they have no known competing financial interests or personal relationships that could have appeared to influence the work reported in this paper.

Acknowledgments

The authors gratefully acknowledge the anonymous reviewers whose thoughtful feedback greatly improved the quality of this manuscript.

Appendix A. Friction formulations

In this annex, the friction formulations briefly introduced in Section 2.3 are explained in more detail.

A.1. Local plasticity approach

The local plasticity approach is based on imposing a limit condition on the frictional stresses in Eq. (20) under a local flow rule. To isolate these $\boldsymbol{\sigma}_i^\mu$ frictional stresses, it is important to first highlight that $\mathbb{H}_i^\circ$ is rank deficient (in the case of penny cracks). This is directly related to the fact that flat cracks have only two independent principal components (one associated with the normal direction and one with the tangential direction). A consequence of this deficiency is that the $\mathbb{H}_i^\circ$ tensors do not have a traditional inverse. Hence, some preparation is needed. First, Eq. (20) can be equally written as:

$$\boldsymbol{\epsilon}_i^c = \mathcal{E}_i \mathbb{H}_i^\circ : \left[\left(\mathbb{N}_i + \mathbb{L}_i \right) : \boldsymbol{\Sigma} - \boldsymbol{\sigma}_i^\mu \right] \tag{52}$$

where $\mathbb{N}_i$ and $\mathbb{L}_i$ are projection tensors[3] that isolate the normal and lateral components of the macro stress $\boldsymbol{\Sigma}$ with respect to the ith crack surface. The two expressions are the same, since the $\mathbb{H}_i^\circ$ tensors already belong to the same space as $\mathbb{L}_i + \mathbb{N}_i$. Hence, the contraction operation leaves the $\mathbb{H}_i^\circ$ tensors unmodified by the unitary and orthogonal projection tensors. However, $\boldsymbol{\sigma}_i^\mu$ can now be correctly isolated as:

$$\boldsymbol{\sigma}_i^\mu = \left(\mathbb{N}_i + \mathbb{L}_i \right) : \boldsymbol{\Sigma} - \frac{1}{\mathcal{E}_i} (\mathbb{H}_i^\circ)^+ \boldsymbol{\epsilon}_i^c \tag{53}$$

where the $\{\cdot\}^+$ operator is the Moore–Penrose inverse.[4]

Similar expressions for $\boldsymbol{\sigma}_i^\mu$ are derived by a different rationalization in several works of Zhu and collaborators (Refs. [17,18,47,51], to cite a few), albeit without the $\mathbb{N}_i + \mathbb{L}_i$ term added in this work for dimensional consistency, and with a regular, rather than pseudoinverse. The frictional stress $\boldsymbol{\sigma}_i^\mu$ can then be made to satisfy the local yield condition, often Coulomb friction. If the crack is found to be sliding (the yield condition is violated), the crack strains can be updated as:

$$\Delta \boldsymbol{\epsilon}_i^c = \Delta \lambda_i^\mu \boldsymbol{G}_i^\mu \tag{54}$$

where $\boldsymbol{G}_i^\mu$ is the flow direction and $\Delta\lambda_i^\mu$ the plastic multiplier. The value of the plastic multiplier can be found by solving a linear complementarity problem in the form:

$$f_i^\mu \le 0 \qquad \Delta\lambda_i^\mu \ge 0 \qquad f_i^\mu \Delta\lambda_i^\mu = 0 \tag{55}$$

As for the sliding direction $\boldsymbol{G}_i^\mu$, it is a function of the fictional stress $\boldsymbol{\sigma}_i^\mu$. An example of this tensor for a Coulomb-like plastic potential can be found in Ref. [47]. In this format, the problem is both fully implicit at the local level and coupled at the global level by the macrostress acting a back-stress term in all the local frictional stresses.

A.2. Stress-rate-based approximation

In the Los Alamos stress-rate formulation, Coulomb friction with no dilatancy is considered. In this case, the rate of change of the crack strains for sliding cracks can be approximated as a linear combination of the friction-locked case (where there is no crack strain rate) and the frictionless sliding case (where the shear component of the crack strain rate is the same as that of an open crack). The scaling factor for this linear combination can be calculated as [6,48]:

$$\eta_i^\mu = \left\langle 1 - \frac{\mu \langle -\sigma_i^N \rangle}{\sigma_i^T} \right\rangle \tag{56}$$

where σ_i^N is the (signed) value of the normal component of the projection of the macroscopic stress tensor $\boldsymbol{\Sigma}$ on the plane of the ith crack family, with σ_i^T being the magnitude of shear component.

The meaning of the η_i^μ scaling factor can be interpreted rather simply: when the shear component of the traction acting on the crack family (term in the denominator) does not exceed the frictional limit on the crack stress (term on the numerator), then $\eta_i^\mu = 0$. On the other hand, when the normal traction component is non-negative, and therefore friction is null, then $\eta_i^\mu = 1$. For intermediate cases, where friction exists, but is less then the shear traction, η_i^μ will assume intermediate values that are directly related to the

[3] The specific format for these tensors and their meaning can be found in Refs. [19,47,51,110,111].

[4] Often called 'pseudoinverse', it is applicable to rank deficient matrices and acts as a 'weak' inverse, such that $\boldsymbol{A}\boldsymbol{A}^+\boldsymbol{A} = \boldsymbol{A}$ and $\boldsymbol{A}^+\boldsymbol{A}\boldsymbol{A}^+ = \boldsymbol{A}^+$.

ratios between these two quantities. Hence, η_i^μ acts as a measure of the portion on the shear traction that is cancelled by friction for ith crack family. With this metric at hand, generalized $\mathbb{H}_i^c$ tensors can be defined as:

$$\mathbb{H}_i^c = H\left(\sigma_i^N\right)\mathbb{H}_i^\circ + H\left(-\sigma_i^N\right)\eta_i^\mu \mathbb{H}_i^* \tag{57}$$

where H is the 'Heaviside step function' and a convention that $H(x) = 1 - H(-x)$ is used. Because of η_i^μ, $\mathbb{H}_i^c$ is a non-linear function of the macroscopic stress tensor, in contrast to the open and frictionless sliding cases, where it is purely a step function. The latter is recovered by setting $\mu = 0$, which always gives $\eta_i^\mu = 1$. In this case (of no friction), then $\mathbb{H}_i^c = \mathbb{H}_i^{*|\circ}$, where the latter tensor assumes either the open ($\circ$) or closed and frictionless ($*$) form depending on the sign of the normal component of the traction on the cracks in the ith family. When the normal component is zero, using $\mathbb{H}_i^\circ$ or $\mathbb{H}_i^*$ yields the same solution, so any of the two formats can be used.

With the $\mathbb{H}_i^c$ tensor at hand, the crack strain rate is then written exclusively in terms of the stress tensor and its rate as:

$$\dot{\epsilon}_i^c = \mathbb{H}_i^c : \dot{\boldsymbol{\Sigma}} \tag{58}$$

This renders the local problem fully explicit. However, friction is now solved only approximately, since the LCP is no longer strictly enforced. As for the global problem, $\boldsymbol{\Sigma}$ is still implicitly-defined. In the SCRAM model, this dependency is addressed by means of an explicit time-integration scheme, thus rendering the whole solution process also explicit.

A.3. Strain-based formulation

An example of a strain-based friction formulation is the one included in the model by Jefferson and Bennett [49,50], which relies on a change of damage variable. It can be readily observed that the compliance tensor for the MT estimate (Table 2) remains finite for any (also finite) value of $\mathcal{E}_i$ (in the case of flat, volumeless penny-shaped cracks). Therefore, $0 \le \mathcal{E}_i < \infty$ and the density parameter has no upper bound in the MT estimate. In order to have a normalized damage variable, Jefferson and Bennett make the substitution:

$$\mathcal{E}_i = k_\nu \frac{\omega_i}{1-\omega_i} \quad ; \quad k_\nu = \frac{3}{16(1-\nu^2)} \tag{59}$$

where the new damage variable ω_i is bounded, since when $\omega_i \to 1$, then $\mathcal{E}_i \to \infty$. Notably, this transformation is defined for an isotropic matrix, since k_ν depends on the Poisson's ratio of the matrix phase ν. Under this transformation, ω_i now carries the meaning of an effective area from Continuum-Damage Mechanics.

Introducing the notations:

$$\mathbb{D}_i^{\omega\circ} = k_\nu \mathbb{H}_i^\circ \quad ; \quad \boldsymbol{\sigma}_i^c = (\mathbb{N}+\mathbb{L}) : \boldsymbol{\Sigma} - \boldsymbol{\sigma}_i^\mu \tag{60}$$

with $\boldsymbol{\sigma}_i^\mu$ again being the local frictional stress, and $\mathbb{N}$ and $\mathbb{L}$ the projection tensors used in Eq. (53), then the individual crack-strain contributions in Eq. (20) can be written, using the transformed damage variable, as:

$$\boldsymbol{\epsilon}_i^c = \frac{\omega_i}{1-\omega_i}\mathbb{D}_i^{\omega\circ}\boldsymbol{\sigma}_i^c \tag{61}$$

Jefferson and Bennett then introduce a so-called 'Equivalent Local Strain'[5] as:

$$\boldsymbol{\epsilon}_i^L = \boldsymbol{\epsilon}_i^{Le} + \boldsymbol{\epsilon}_i^c \quad ; \quad \boldsymbol{\epsilon}_i^{Le} = \mathbb{D}_i^{\omega\circ} : \boldsymbol{\sigma}_i^c \tag{62}$$

where $\boldsymbol{\epsilon}_i^{Le}$ is the elastic part of this local strain. Then, instead of isolating the frictional stresses σ_i^μ and having them satisfy a stress-based yield condition, Jefferson and Bennett propose an explicit expression for this contribution of form:

$$\boldsymbol{\sigma}_i^\mu = \omega_i \alpha_i^\mu \mathbb{C}_i^{\omega\circ} : \mathbb{G}_i^\mu : \boldsymbol{\epsilon}_i^L \tag{63}$$

whose terms will be discussed later. With the frictional stress explicitly written in terms of the local strains, the latter can be fully isolated, leading to

$$\boldsymbol{\epsilon}_i^L = \mathbb{D}_i^L : \boldsymbol{\Sigma} \quad ; \quad \mathbb{D}_i^L = \left[(1-\omega_i)\mathbb{I} + \alpha_i^\mu \omega_i \mathbb{G}_i^\mu\right]^{-1} : \mathbb{D}_i^{\omega\circ} \tag{64}$$

If a local compliance tensor is then defined as:

$$\mathbb{D}_i^L = \mathbb{D}_i^{\omega\circ} + \mathbb{D}_i^c \tag{65}$$

it follows that the *additional* local compliance due to the presence of a crack family can be written as:

$$\mathbb{D}_i^c = \left\{\left[(1-\omega_i)\mathbb{I} + \alpha_i^\mu \omega_i \mathbb{G}_i^\mu\right]^{-1} - \mathbb{I}\right\} : \mathbb{D}_i^{\omega\circ} \tag{66}$$

This tensor can be used to calculate the homogenized compliance for the MT estimate using the expression in Table 2 in place of $\mathcal{E}_i\mathbb{H}_i^\circ$. More importantly, it can also be used to calculate the homogenized stiffness from the same table, using the relationship

[5] A vector in the original paper, here expressed, equivalently, as a tensor.

between $\mathbb{M}$ and $\mathbb{H}$ from Eq. (10). However, to do so, $\mathbb{D}_i^c$ needs to be scaled by an integration weight in both cases. The reasoning from this is explained in Section 3.3.

In the stress-based formulations, the state of the crack family (open, sliding, or friction-locked) is determined by the sign of the normal stress to and the yield function. In the model by Jefferson and Bennett, on the other hand, two functions of the strain components are written, namely:

$$\phi_i^\mu = 2m_g\epsilon_i^{L,N} - \epsilon_i^{L,T} \quad ; \quad \phi_i^l = \epsilon_i^{L,N} + 2m_g\epsilon_i^{L,T} \tag{67}$$

where $\epsilon_i^{L,N}$ and $\epsilon_i^{L,T}$ are the normal and shear components of the local strain projected on the crack plane. These components are then forced to be the same as the components of the macroscopic strain projected on the crack plane, hence establishing the macro-to-local link. These ϕ_i^μ and ϕ_i^l functions then form two perpendicular lines in $\left(\epsilon_i^{L,T}, \epsilon_i^{L,N}\right)$ space, $\phi_i^\mu = 0$ being the sliding boundary, and $\phi_i^l = 0$ the locking one. This choice is based on a geometrical argument of cone-like crack asperities, which was illustrated first in Refs. [112,113] in the context of the damage-plastic 'Craft' model, and later in Refs. [49,50] in the micromechanical context employed here. The three crack states are then set based on the regions defined by these two lines and the $\epsilon_i^{L,T} = 0$ axis. More explicitly, since the tangential strain component cannot be negative ($\epsilon_i^{L,T} \geq 0$), the conditions are:

$$\text{Crack state} = \begin{cases} \text{Open} & \text{If} \quad \epsilon_i^{L,N} > 0 \wedge \phi_i^\mu > 0 \\ \text{Locked} & \text{If} \quad \epsilon_i^{L,N} < 0 \wedge \phi_i^l < 0 \\ \text{Sliding} & \text{Otherwise} \end{cases} \tag{68}$$

where $\wedge$ is the logical 'and' operator.

One notable aspect of this formulation is that, contrarily to the stress-based formulations previously discussed, the one by Jefferson and Bennett allows for a frictional response even when $\epsilon_i^{L,N}$ is positive, as long as the tangential component is sufficiently large to ensure that ϕ_i^μ is negative, which again has a geometrical meaning, since contact between peaks of the two rough surfaces is possible with sufficient sliding, even under positive normal separation between them. This behavior is determined by the $\mathbb{G}$ tensor, which was introduced in by Jefferson in Ref. [112] and is a central aspect of the damage-plastic 'Craft' model [112–114]. Nevertheless, with increasing (positive) normal strain components, the contact area between the two opposite surfaces will decrease, which will reduce the stresses that can be transferred between the crack surfaces. This is achieved by the α_i^μ scaling parameter in Eq. (63), whose format can be seen in Ref. [49,75,76,78].

Finally, as for the $\mathbb{G}_i^\mu$ tensor in Eq. (63), it follows from the same geometrical argument of cone-like surface asperities and involves first and second-order derivatives of the ϕ_i^μ scalars with respect to the local strains.

Appendix B. Damage evolution in the model by Jefferson and Bennett

In the original formulation of Jefferson and Bennett [49], the driving force is written as:

$$\mathcal{F}_i = \frac{\epsilon_i^N}{2}\left[1 + \left(\frac{\mu_d}{k_s}\right)^2 \left(\epsilon_i^T\right)^2\right] + \frac{1}{2k_s^2}\sqrt{\left(k_s^2 - \mu_d^2\right)^2 \left(\epsilon_i^N\right)^2 + \left(4k_s\epsilon_i^T\right)^2} \tag{69}$$

where $\mu_d = E/G = 2(1+\nu)$ and $k_s = k_f\mu_d$, with $k_f = f_s/f_t$. The input parameters are f_s, the shear strength, and f_t, the tensile one.

As mentioned in Section 3.3, the resistance function is simply:

$$\mathcal{R}_i = \zeta_i \tag{70}$$

where ζ_i can be understood as an effective (local) strain scalar. This scalar starts as the tensile strain limit $\epsilon_{t0} = f_t/E$, with $k_s\zeta_i$ being the shear strain limit. When damage evolves, the limit surface enlarges (since a larger strain is needed to trigger further damage evolution).

The connection between ζ_i and the damage parameters ω_i is written as [49,50,75]:

$$\omega_i = 1 - \frac{\epsilon_{t0}}{\zeta_i}\exp\left(-k_w\frac{\zeta_i - \epsilon_{t0}}{\epsilon_{tu} - \epsilon_{t0}}\right) \tag{71}$$

where with ϵ_{tu} being the ultimate tensile strain (strain at complete loss of cohesion). k_w is a fit constant that adjusts the rate of softening, normally set be the authors as 5 [49,50,75,77]. The meaning of the damage parameters ω_i is related to the friction formulation discussed in Annex A.3.

Data availability

Data will be made available on request.

References

[1] Dormieux L, Lemarchand E, Kondo D, Fairbairn E. Elements of poro-micromechanics applied to concrete. Mater Struct 2004;37(1):31–42.
[2] Esposito R, Hendriks MA. A multiscale micromechanical approach to model the deteriorating impact of alkali-silica reaction on concrete. Cem Concr Compos 2016;70:139–52.
[3] Iskhakov T, Timothy JJ, Meschke G. Expansion and deterioration of concrete due to asr: Micromechanical modeling and analysis. Cem Concr Res 2019;115:507–18.
[4] Wu W, Zhao L, Lai Y, Lv Z, Chen Y, Ran J. A rational multiscale nonlinear constitutive model for freeze–thaw rocks under triaxial compression. Int J Plast 2024;179:104040.
[5] Yang K, Wu Y, Huang F. Numerical simulations of microcrack-related damage and ignition behavior of mild-impacted polymer bonded explosives. J Hazard Mater 2018;356:34–52.
[6] Dienes J, Zuo Q, Kershner J. Impact initiation of explosives and propellants via statistical crack mechanics. J Mech Phys Solids 2006;54(6):1237–75.
[7] Yu Q, Du S, Zhu Q, Luo Z, Liu S, Zhao L. An extended micromechanical-based plastic damage model for understanding water effects on quasi-brittle rocks. Int J Min Sci Technol 2024;34(3):289–304.
[8] Dormieux L, Kondo D, Ulm F-JF-J. Microporomechanics. Wiley; 2006.
[9] Jiang T, Shao J, Xu W, Zhou C. Experimental investigation and micromechanical analysis of damage and permeability variation in brittle rocks. Int J Rock Mech Min Sci 2010;47(5):703–13.
[10] Ulloa J, Noii N, Alessi R, Aldakheel F, Degrande G, François S. Variational modeling of hydromechanical fracture in saturated porous media: A micromechanics-based phase-field approach. Comput Methods Appl Mech Engrg 2022;396:115084.
[11] Zhu Q-Z, Yuan S-S, Shao J-F. Microporomechanics of quasi-brittle rocks: Theoretical formulations and analytical simulations. Int J Plast 2023;171:103789.
[12] Goidescu C, Welemane H, O. Pantalé M Karama, Kondo D. Anisotropic unilateral damage with initial orthotropy: A micromechanics-based approach. Int J Damage Mech 2015;24(3):313–37.
[13] Qi M, Shao J, Giraud A, Zhu Q, Colliat J. Damage and plastic friction in initially anisotropic quasi brittle materials. Int J Plast 2016;82:260–82.
[14] Zhou Y, Sluijs LJ, Esposito R. A microporomechanical model to predict nonlinear material behavior of masonry. CRC Press; 2022, p. 363–72.
[15] Pensée V, Kondo D, Dormieux L. Micromechanical analysis of anisotropic damage in brittle materials. J Eng Mech 2002;128(8):889–97.
[16] Zhu QZ, Kondo D, Shao JF. Homogenization-based analysis of anisotropic damage in brittle materials with unilateral effect and interactions between microcracks. Int J Numer Anal Methods Geomech 2009;33(6):749–72.
[17] Zhu Q, Kondo D, Shao J, Pensee V. Micromechanical modelling of anisotropic damage in brittle rocks and application. Int J Rock Mech Min Sci 2008;45:467–77.
[18] Zhu QZ, Kondo D, Shao JF. Micromechanical analysis of coupling between anisotropic damage and friction in quasi brittle materials: Role of the homogenization scheme. Int J Solids Struct 2008;45:1385–405.
[19] Zhu QZ, Zhou CB, Shao JF, Kondo D. A discrete thermodynamic approach for anisotropic plastic-damage modeling of cohesive-frictional geomaterials. Int J Numer Anal Methods Geomech 2010;34:1250–70.
[20] Ulloa J, Wambacq J, Alessi R, Samaniego E, Degrande G, François S. A micromechanics-based variational phase-field model for fracture in geomaterials with brittle-tensile and compressive-ductile behavior. J Mech Phys Solids 2022;159:104684.
[21] Zhao L-Y, Ren L, Liu L-H, Lai Y-M, Niu F-J, You T. Multiscale modeling of diffuse damage and localized cracking in quasi-brittle materials under compression with a quadratic friction law. Int J Solids Struct 2024;304:113038.
[22] Kachanov M. Elastic solids with many cracks and related problems. Advances in applied mechanics, vol. 30, Elsevier; 1993, p. 259–445.
[23] Kachanov M, Sevostianov I. Micromechanics of materials, with applications, vol. 249, Springer; 2018.
[24] Hill R. A self-consistent mechanics of composite materials. J Mech Phys Solids 1965;13(4):213–22.
[25] Mura T. Micromechanics of defects in solids. In: Mechanics of elastic and inelastic solids. Springer Netherlands; 1987.
[26] Nemat-Nasser S, Hori M. Micromechanics: overall properties of heterogeneous materials. North-holland series in applied mathematics and mechanics, Vol. 37, Elsevier; 1995.
[27] Mori T, Tanaka K. Average stress in matrix and average elastic energy of materials with misfitting inclusions. Acta Metall 1973;21(5):571–4.
[28] Benveniste Y. On the mori-tanaka's method in cracked bodies. Mech Res Commun 1986;13(4):193–201.
[29] Benveniste Y. A new approach to the application of mori-tanaka's theory in composite materials. Mech Mater 1987;6(2):147–57.
[30] Castañeda PP, Willis JR. The effect of spatial distribution on the effective behavior of composite materials and cracked media. J Mech Phys Solids 1995;43(12):1919–51.
[31] Eshelby JD, Peierls RE. The determination of the elastic field of an ellipsoidal inclusion, and related problems. Proc R Soc Lond Ser A 1957;241(1226):376–96.
[32] Bristow JR. Microcracks, and the static and dynamic elastic constants of annealed and heavily cold-worked metals. Br J Appl Phys 1960;11(2):81.
[33] Budiansky B, O'connell RJ. Elastic moduli of a cracked solid. Int J Solids Struct 1976;12(2):81–97.
[34] Horii H, Nemat-Nasser S. Overall moduli of solids with microcracks: load-induced anisotropy. J Mech Phys Solids 1983;31(2):155–71.
[35] Dormieux L, Kondo D. Poroelasticity and damage theory for saturated cracked media. Vienna: Springer Vienna; 2005, p. 153–86.
[36] Böhm HJ. A short introduction to basic aspects of continuum micromechanics. Tech. rep. ILSB report 206, Vienna, Austria: Institute of Lightweight Design and Structural Biomechanics, TU Wien; 2024.
[37] Hu G, Weng G. The connections between the double-inclusion model and the ponte castaneda–willis, mori–tanaka, and kuster–toksoz models. Mech Mater 2000;32(8):495–503.
[38] Dormieux L, Kondo D. Stress-based estimates and bounds of effective elastic properties: The case of cracked media with unilateral effects. Comput Mater Sci 2009;46(1):173–9.
[39] V. Deudé L Dormieux, Kondo D, Pensée V. Propriétés élastiques non linéaires d'un milieu mésofissuré. C R Méc 2002;330(8):587–92.
[40] Prat PC, Bažant ZP. Tangential stiffness of elastic materials with systems of growing or closing cracks. J Mech Phys Solids 1997;45(4):611–36.
[41] Jin W, Arson C. Micromechanics based discrete damage model with multiple non-smooth yield surfaces: Theoretical formulation, numerical implementation and engineering applications. Int J Damage Mech 2018;27(5):611–39.
[42] Iskhakov T, Giebson C, Timothy JJ, Ludwig HM, Meschke G. Deterioration of concrete due to asr: Experiments and multiscale modeling. Cem Concr Res 2021;149:106575.
[43] Vu G, Diewald F, Timothy JJ, Gehlen C, Meschke G. Reduced order multiscale simulation of diffuse damage in concrete. Materials 2021;14(14).
[44] Shao JF, Zhou H, Chau KT. Coupling between anisotropic damage and permeability variation in brittle rocks. Int J Numer Anal Methods Geomech 2005;29(12):1231–47.
[45] Shao J, Chau K, Feng X. Modeling of anisotropic damage and creep deformation in brittle rocks. Int J Rock Mech Min Sci 2006;43(4):582–92.
[46] Zhu Q, Shao J, Mainguy M. A micromechanics-based elastoplastic damage model for granular materials at low confining pressure. Int J Plast 2010;26(4):586–602.
[47] Zhu QZ, Shao JF. A refined micromechanical damage-friction model with strength prediction for rock-like materials under compression. Int J Solids Struct 2015;60:75–83.

[48] Zuo QH, Dienes JK, Middleditch J, Meyer J, W H. Modeling anisotropic damage in an encapsulated ceramic under ballistic impact. J Appl Phys 2008;104(2):023508.
[49] Jefferson AD, Bennett T. Micro-mechanical damage and rough crack closure in cementitious composite materials. Int J Numer Anal Methods Geomech 2007;31(2):133–46.
[50] Jefferson A, Bennett T. A model for cementitious composite materials based on micro-mechanical solutions and damage-contact theory. Comput Struct 2010;88(23):1361–6, Special Issue: Association of Computational Mechanics – United Kingdom..
[51] Zhu QZ, Shao JF, Kondo D. A micromechanics-based thermodynamic formulation of isotropic damage with unilateral and friction effects. Eur J Mech A Solids 2011;30:316–25.
[52] Zhao L-Y, Lai Y-M, Shao J-F, Zhang W-L, Zhu Q-Z, Niu F-J. Friction-damage coupled models and macroscopic strength criteria for ice-saturated frozen silt with crack asperity variation by a micromechanical approach. Eng Geol 2021;294:106405.
[53] Zhao L-Y, Lv Z-M, Lai Y-M, Zhu Q-Z, Shao J-F. A new micromechanical damage model for quasi-brittle geomaterials with non-associated and state-dependent friction law. Int J Plast 2023;165:103606.
[54] Xie N, Zhu Q-Z, Shao J-F, Xu L-H. Micromechanical analysis of damage in saturated quasi brittle materials. Int J Solids Struct 2012;49(6):919–28.
[55] Hu K, Shao J-F, Zhu Q-Z, Zhao L-y, Wang W, Wang R-B. A micro-mechanics-based elastoplastic friction-damage model for brittle rocks and its application in deformation analysis of the left bank slope of jinping i hydropower station. Acta Geotech 2020;15:3443–60.
[56] Hu K, Zhang C, Zhu Q, Chen X, Liu S, Wu J, Li R. A time-dependent damage constitutive model for brittle rock materials based on subcritical damage theory. ACS Omega 2024;9(30):32579–92.
[57] Liu S-L, Zhu Q-Z, Zhao L-Y, Yu Q-J, Zhang J, Cao Y-J. Experimental investigation and micromechanics-based constitutive modeling of the transition from brittle to ductile behavior in saturated low-porosity rocks. Appl Math Model 2024;126:506–25.
[58] Liu S, Zhu Q, Zhang J. Multi-scale constitutive modeling of the brittle–ductile transition behavior of rocks with microcracks and two populations of pores. Geomech Energy Environ 2024;40:100591.
[59] Tong F, Zhang J, Zhu Q-Z, Du J, Shao J. Micromechanical modeling and simulation of instantaneous and long-term behaviors of red sandstone under lateral unloading conditions. Rock Mech Rock Eng 2024;57:9097–120.
[60] Ren L, Lv Z-M, Niu F-J, Qin Z-P, Zhao L-Y. A novel three dimensional failure criterion for quasi-brittle materials based on multi-scale damage approach. Mech Mater 2024;198:105142.
[61] V. Deudé L Dormieux, Kondo D, Maghous S. Micromechanical approach to nonlinear poroelasticity: Application to cracked rocks. J Eng Mech 2002;128(8):848–55.
[62] Zhao L, Zhu Q, Xu W, Dai F, Shao J. A unified micromechanics-based damage model for instantaneous and time-dependent behaviors of brittle rocks. Int J Rock Mech Min Sci 2016;84:187–96.
[63] Esposito R. The deteriorating impact of alkali-silica reaction on concrete: Expansion and mechanical properties (Ph.D. thesis), Delft University of Technology; 2016.
[64] Zhu Q, Shao J. Micromechanics of rock damage: Advances in the quasi-brittle field. J Rock Mech Geotech Eng 2017;9(1):29–40.
[65] Mazars J. A description of micro- and macroscale damage of concrete structures. Eng Fract Mech 1986;25(5):729–37.
[66] Lanoye E, Dormieux L, Kondo D. A micromechanical-based damage analysis of a cylindrical bar under torsion: Theoretical results, finite elements verification and application. Theor Appl Fract Mech 2014;74:116–25.
[67] Zhao L-Y, Zhu Q-Z, Shao J-F. A micro-mechanics based plastic damage model for quasi-brittle materials under a large range of compressive stress. Int J Plast 2018;100:156–76.
[68] Keer L. A note on shear and combined loading for a penny-shaped crack. J Mech Phys Solids 1966;14(1):1–6.
[69] Dienes JK. On the stability of shear cracks and the calculation of compressive strength. J Geophys Res: Solid Earth 1983;88(B2):1173–9.
[70] Rice JR. Comments on ‘‘on the stability of shear cracks and the calculation of compressive strength’’ by jk dienes. J Geophys Res: Solid Earth 1984;89(B4):2505–7.
[71] Zuo Q, Addessio F, Dienes J, Lewis M. A rate-dependent damage model for brittle materials based on the dominant crack. Int J Solids Struct 2006;43(11):3350–80.
[72] Deganis LE, Zuo QH. Crack-mechanics based brittle damage model including nonlinear equation of state and porosity growth. J Appl Phys 2011;109(7):073504.
[73] Zuo QH, Deganis LE, Wang G. Elastic waves and damage quantification in brittle material with evolving damage. J Phys D: Appl Phys 2012;45(14):145302.
[74] Kunin A, Zuo Q. Stability and well-posedness of a rate-dependent damage model for brittle materials based on crack mechanics. Appl Math Model 2016;40(5):3801–11.
[75] Mihai I, Jefferson A. A material model for cementitious composite materials with an exterior point eshelby microcrack initiation criterion. Int J Solids Struct 2011;48(24):3312–25.
[76] Mihai I, Jefferson A. Smoothed contact in a micromechanical model for cement bound materials. Comput Struct 2013;118:115–25, Special Issue: UK Association for Computational Mechanics in Engineering..
[77] Mihai IC, Jefferson AD. A micromechanics based constitutive model for fibre reinforced cementitious composites. Int J Solids Struct 2017;110–111:152–69.
[78] Mihai I, Jefferson A, Lyons P. Micromechanics based modelling of fibre reinforced cementitious composites. In: Computational modelling of concrete structures. CRC Press; 2018, p. 895–901.
[79] Shen L, Li J. A numerical simulation for effective elastic moduli of plates with various distributions and sizes of cracks. Int J Solids Struct 2004;41(26):7471–92.
[80] Kushch V, Sevostianov I, Mishnaevsky L. Effect of crack orientation statistics on effective stiffness of mircocracked solid. Int J Solids Struct 2009;46(6):1574–88.
[81] Feng X-Q, Yu S-W. Damage micromechanics for constitutive relations and failure of microcracked quasi-brittle materials. Int J Damage Mech 2010;19(8):911–48.
[82] Charpin L, Ehrlacher A. Estimating the poroelastic properties of cracked materials. Acta Mech 2014;225(9):2501–19.
[83] J. Bluthé B Bary, Lemarchand E. Closure of parallel cracks: Micromechanical estimates versus finite element computations. Eur J Mech A Solids 2020;81:103952.
[84] J. Bluthé B Bary, Lemarchand E. Contribution of fe and fft-based methods to the determination of the effective elastic and conduction properties of composite media with flat inclusions and infinite contrast. Int J Solids Struct 2021;216:108–22.
[85] Vasylevskyi K, Drach B, Tsukrov I. On micromechanical modeling of orthotropic solids with parallel cracks. Int J Solids Struct 2018;144–145:46–58.
[86] Saenger EH, Krüger OS, Shapiro SA. Effective elastic properties of randomly fractured soils: 3d numerical experiments. Geophys Prospect 2004;52(3):183–95.
[87] Hashin Z. The differential scheme and its application to cracked materials. J Mech Phys Solids 1988;36(6):719–34.
[88] Markov KZ. On the cluster bounds for the effective properties of microcracked solids. J Mech Phys Solids 1998;46(2):357–88.
[89] González JM Ortolano, Ortega JA Hernández, Olivella X Oliver. A comparative study on homogenization strategies for multi-scale analysis of materials. Centre Internacional de Mètodes Numèrics en Enginyeria (CIMNE); 2013.
[90] Klusemann B, Svendsen B. Homogenization methods for multi-phase elastic composites: Comparisons and benchmarks. Tech Mech-Eur J Eng Mech 2010;30(4):374–86.

[91] Dormieux L, Kondo D. Micromechanics of fracture and damage. John Wiley & Sons; 2016.
[92] Qi M, Shao JF, Giraud A, Zhu QZ, Colliat JB. Damage and plastic friction in initially anisotropic quasi brittle materials. Int J Plast 2016;82:260–82.
[93] Gao H, Rice JR. Somewhat circular tensile cracks. Int J Fract 1987;33(3):155–74.
[94] Gol'dstein RV, Salganik RL. Brittle fracture of solids with arbitrary cracks. Int J Fract 1974;10:507–23.
[95] Cotterell B, Rice JR. Slightly curved or kinked cracks. Int J Fract 1980;16:155–69.
[96] Erdogan F, Sih GC. On the crack extension in plates under plane loading and transverse shear. J Basic Eng 1963;85(12):519–25.
[97] Williams JG, Ewing PD. Fracture under complex stress — the angled crack problem. Int J Fract Mech 1972;8:441–6.
[98] Adams M, Sines G. Crack extension from flaws in a brittle material subjected to compression. Tectonophysics 1978;49(1):97–118.
[99] Cannon N, Schulson E, Smith T, Frost H. Wing cracks and brittle compressive fracture. Acta Met Mater 1990;38(10):1955–62.
[100] Germanovich LN, Salganik RL, Dyskin AV, Lee KK. Mechanisms of brittle fracture of rock with pre-existing cracks in compression. Pure Appl Geophys 1994;143:117–49.
[101] Dyskin A, Jewell R, Joer H, Sahouryeh E, Ustinov K. Experiments on 3-d crack growth in uniaxial compression. Int J Fract 1994;65:R77–83.
[102] Dyskin A, Sahouryeh E, Jewell R, Joer H, Ustinov K. Influence of shape and locations of initial 3-d cracks on their growth in uniaxial compression. Eng Fract Mech 2003;70(15):2115–36.
[103] Yin P, Wong R, Chau K. Coalescence of two parallel pre-existing surface cracks in granite. Int J Rock Mech Min Sci 2014;68:66–84.
[104] Kachanov ML. A microcrack model of rock inelasticity part ii: Propagation of microcracks. Mech Mater 1982;1(1):29–41.
[105] Fanella D, Krajcinovic D. A micromechanical model for concrete in compression. Eng Fract Mech 1988;29(1):49–66.
[106] Lee X, Ju JW. Micromechanical damage models for brittle solids. part ii: Compressive loadings. J Eng Mech 1991;117(7):1515–36.
[107] Lehner F, Kachanov M. On modelling of 'winged' cracks forming under compression. Int J Fract 1996;77:R69–75.
[108] Basista M, Gross D. The sliding crack model of brittle deformation: An internal variable approach. Int J Solids Struct 1998;35(5):487–509.
[109] Dyskin AV, Germanovich LN, Ustinov KB. A 3-d model of wing crack growth and interaction. Eng Fract Mech 1999;63(1):81–110.
[110] Yu Q, Du S, Zhu Q-Z, Shao J-F, Yong R. A novel micro-mechanical anisotropic elastic–plastic damage model for understanding time-dependent behaviors on rock-like materials. Int J Rock Mech Min Sci 2024;179:105780.
[111] Zhang J, Liu W, Yu Q, Zhu Q-Z, Shao J-F. A micromechanical model for induced anisotropic damage-friction in rock materials under cyclic loading. Int J Rock Mech Min Sci 2025;186:106014.
[112] Jefferson AD. Constitutive modelling of aggregate interlock in concrete. Int J Numer Anal Methods Geomech 2002;26(5):515–35.
[113] Jefferson A. Craft—-a plastic-damage-contact model for concrete. i. model theory and thermodynamic considerations. Int J Solids Struct 2003;40(22):5973–99.
[114] Mihai IC, Jefferson AD, Lyons P. A plastic-damage constitutive model for the finite element analysis of fibre reinforced concrete. Eng Fract Mech 2016;159:35–62.